MATERIALS CHEMISTRY FRONTIERS

REVIEW

View Article Online
View Journal | View Issue

Cite this: *Mater. Chem. Front.*, 2023, 7, 2973

Visualizing intracellular dynamics with AIE probes

Michelle M. S. Lee,†[a] Eric Y. Yu,†[a] Joe H. C. Chau,[a] Jacky W. Y. Lam,[a] Ryan T. K. Kwok,*[a] Dong Wang *[b] and Ben Zhong Tang*[c]

Received 31st December 2022,
Accepted 17th March 2023

DOI: 10.1039/d2qm01382g

rsc.li/frontiers-materials

As a sensitive, selective, and non-invasive method, fluorescence bioimaging stands out in biological and pathological studies to visualize biological processes on the microscale. However, the initial photophysical property of conventional organic fluorophores leads to poor photostability and a low signal-to-noise ratio, which largely hinder their performance in the long-term monitoring and tracing of intracellular processes. In contrast, AIE luminogens (AIEgens) exhibit opposite photophysical properties that overcome the barrier to facilitate real-time and long-term intracellular dynamics visualization. This work summarizes the recent development of AIE probes to unveil intracellular processes, covering from intracellular microenvironment monitoring to tracing intracellular bioprocesses. As fluorescent bioprobes with AIE features have unlimited potential in bioimaging studies, we hope this review can offer more inspiration and directions for the future design and development of AIEgens for visualizing and monitoring diversified intracellular dynamics.

1. Introduction

Bioimaging is an important method to non-invasively visualize biological processes in real-time, facilitating the studies of biological and pathological processes in living systems from the microscale to the molecular level. Various widely used bioimaging tools include X-ray, computed tomography (CT), magnetic resonance imaging (MRI), positron emission tomography (PET), as well as various types of fluorescence imaging methods, covering super-resolution, two-photon excitation microscopy, fluorescence recovery after photobleaching (FRAP), and fluorescence resonance energy transfer (FRET) technologies.[1] Among them, fluorescence bioimaging stands out in terms of its high sensitivity, high selectivity, imaging method versatility, as well as a unique choice of spatial and temporal resolution.[2,3] In the past few decades, a diverse range of studies have been conducted to develop various useful fluorescent bioimaging probes, including quantum dots, inorganic fluorescent nanoparticles, and metallic nanoclusters.[4–6] Despite their excellent photophysical properties, these fluorescent probes have inherent properties that create challenges in bioimaging applications, in terms of potential cytotoxicity from the heavy metals, size controlled reproduction of nanoparticles or nanoclusters, low nanoprobe loading efficiency, and poor long-term stability in the cell environment.

As such, organic fluorescent dyes have attracted much attention as alternative bioimaging probes.[7–10] Common organic fluorescent dyes include cyanine, fluorescein, and rhodamine. However, conventional organic fluorophores consist of planar structures that exhibit aggregation-caused quenching phenomenon, in which such fluorophores emit strongly in the solution state but suffer from emission quenching in high concentration or the aggregate state under strong π–π stacking.[11] This phenomenon results in poor photostability and a low signal-to-noise ratio in bioimaging studies. Furthermore, to improve the imaging resolution of these organic fluorescent dyes, multiple washing procedures or cell fixation processes are required, which further restrict the bioimaging studies from real-time monitoring and visualization, resulting in imaging inaccuracy with the possibility of omitting certain bioprocesses.

In contrast to ACQ fluorescent dyes, rapidly developed aggregation-induced emission luminogens (AIEgens) have the opposite photophysical properties.[12,13] AIEgens were non-emissive in the solution state under free intramolecular motions. Still, they give strong emissions at high concentration or in the aggregate form, which is attributed to the mechanism of restriction of intramolecular motions (RIMs), including

[a] *Hong Kong Branch of Chinese National Engineering Research Center for Tissue Restoration and Reconstruction, Department of Chemistry, The Hong Kong University of Science and Technology, Clear Water Bay, Kowloon, Hong Kong, 999077, China. E-mail: chryan@ust.hk*
[b] *Centre for AIE Research, Shenzhen Key Laboratory of Polymer Science and Technology, Guangdong Research Center for Interfacial Engineering of Functional Materials, College of Material Science and Engineering, Shenzhen University, Shenzhen 518061, P. R. China. E-mail: wangd@szu.edu.cn*
[c] *School of Science and Engineering, Shenzhen Institute of Aggregate Science and Technology, The Chinese University of Hong Kong, Shenzhen, Guangdong 518172, China. E-mail: tangbenz@cuhk.edu.cn*
† These authors contributed equally to this work.

restriction of intramolecular rotation (RIR) and restriction of intramolecular vibration (RIV). Such opposite emission properties allow AIEgens to perform uniquely in bioimaging applications, exhibiting a high signal-to-noise ratio, high photostability, and a large Stokes shift. In recent years, various AIEgens have been utilized in diversified bioimaging studies and further theranostics applications.[14–17] In particular, a handful of these AIE bioprobes were demonstrated to visualize intracellular dynamics, which shows the significance of AIEgens in biological and biomedical applications. Along with rapid and diversified studies of this field, it is worthwhile to review the recent progress of AIEgens to visualize and monitor intracellular dynamics.

In this work (Scheme 1), we summarize the development of AIE probes to visualize intracellular dynamics, classified into two sections: AIEgens to indicate intracellular microenvironment changes, and AIEgens to facilitate intracellular event tracking and monitoring. In the intracellular microenvironment, reports demonstrating the use of AIE probes to monitor indicators like cellular pH changes, cellular polarity changes, cellular temperature changes, cellular viscosity changes, cellular ROS and hypoxia conditions, and intracellular enzyme and bio-thiol levels were discussed (Table 1). In addition, AIE probes contributing to monitoring and tracking cell apoptosis, drug and gene delivery, cellular response to bacteria entry, intracellular bacteria, mitochondrial changes and mitophagy, and nucleus division are summarized in the second part (Table 2). Finally, conclusions and perspectives of AIE research are illustrated for future studies of AIE probe design and the direction to utilizing intracellular dynamics visualization.

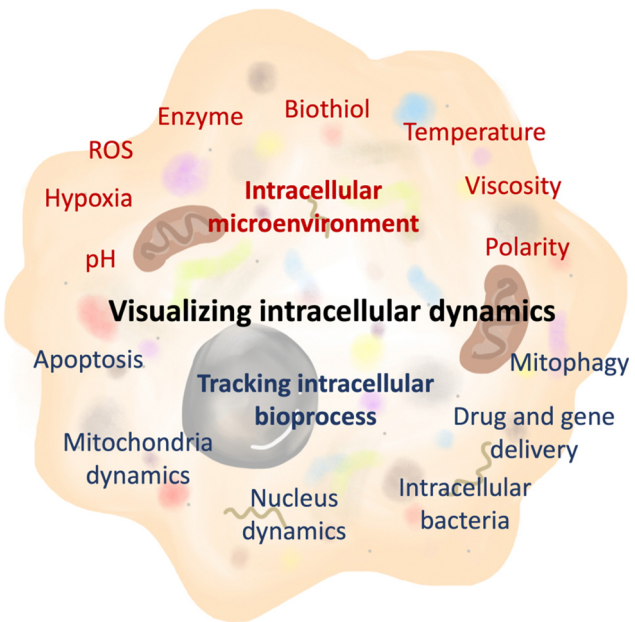

Scheme 1 Schematic diagram of AIE probes in visualizing and tracking various intracellular dynamics.

2. Monitoring and detecting intracellular environment changes

Cellular pH

pH is a measurement for acidity and alkalinity, or the concentration of hydrogen ions, and is an essential aspect of the intracellular environment. Precise regulation is a prerequisite for appropriate cellular function and maintaining homeostasis. As biological cells are full of fluid that acts as a buffer, intracellular pH is dynamic but also well maintained through the action of ion exchangers and pumps in the plasma membrane. Physiologically intracellular pH is kept within a narrow range between 7.0 and 7.4, with slight variation between tissues. Intracellular pH variation across cellular compartments may span from 4.5 to 8.0.[18] The pH difference has significant functional consequences for intracellular organelles. For instance, the lysosome is likely to have a more acidic environment for the digestion and breakdown of proteins, toxins, and other substances. Dysregulation of intracellular pH leads to abnormal cell behavior and is associated with various diseases. The dynamic intracellular pH is usually lower in cancer cells and constitutively decreased in neurodegenerative diseases compared to normal cells.[19] With the dynamic fluctuations of pH inside cells, AIE probes have made it possible to visualize and monitor intracellular pH changes in real-time.

Zhao *et al.* reported a pH-sensitive ratiometric fluorescence probe called LD-L (Fig. 1A).[20] LD-L displays an emission blue-shift upon protonation due to the weakened intracellular charge transfer process. As illustrated in Fig. 1B, LD-L could dynamically monitor the slight changes of pH in HeLa cells. In a neutral environment, LD-L displays a strong red emission only. Upon increasing the acidity in HeLa cells, protonation of LD-L takes place gradually, which can be visualized by the enhanced blue emission and reduced red emission. Tang *et al.* reported an AIE probe to detect an entire pH spectrum from pH 1–14 based on nucleophilic addition reaction.[21] The probe TPE-Cy displays two fluorescence responses with the change of pH value. In the acidic intracellular environment, a strong red emission could be observed. In a basic cellular environment, a blue emission is found. The dual color ratiometric response is attributed to the excellent reactivity with OH^- and H^+. Tang *et al.* reported another pH-responsive ratiometric AIE probe named dhBBR.[22] Interestingly, the reported dhBBR probe not only could visualize pH changes but also reflect cell membrane permeability due to an ion effect. Li *et al.* developed an intracellular pH indicator called Pyr-5, displaying orange and blue emission, respectively, when the pH value is above or below 7 (Fig. 1C).[23] Similarly, Pyr-5 undergoes a weakened intracellular charge transfer effect upon protonation, resulting in a blue-shifted emission. *In situ* monitoring of intracellular pH in HeLa cells shows that Pyr-5 presented orange emission in living cells of pH 7. The orange emission is weakened, and a blue emission appears when pH is reduced to 6. Further increasing the acidity led to a dominant blue emission. Furthermore, the localization of Pyr-5 shifted from the lipid droplets to mitochondria concerning pH changes (Fig. 1D), achieving a

Table 1 Summary of AIE probes for monitoring intracellular environments

AIEgen	Excitation (nm)	Emission (nm)	Feature(s)	Application	Ref.
LD-L	410	475/570	pH 4.0–7.0	Intracellular pH monitoring	20
TPE-Cy	380	485/619	pH 1.0–14.0		21
dhBBR	426	454/511	pH 1.0–12.0		22
Pyr-5	402	450/565	pH 5.0–7.0		23
TPE-DCP	410	615	pH 3.0–12.0		24
TCC	320	440/560	pH 4.0–10.0		25
PNVCL	365/460/535	527/682/674	25–38 °C	Cellular temperature sensing	28
P1	364	520	28–40 °C		29
LCAPU-TPE	320	475	31–45 °C		30
TRF NP	440	680	25–65 °C		31
TICT-lipid	410	508/544/634	Reflect different packing within a bacterial membrane	Cellular polarity	34
IQ-Cm	437	530/585/600	Pathogen discrimination		35
TR-1	410	500	Monitor and differentiate cancer cell progression		36
LDs-BCA	570	650	Monitor cell polarity and dynamic metabolic response		37
CTPA	410/460	456/605	Monitor polarity fluctuation		38
NTPAN-MI	390	560	Quantify subcellular polarity changes		39
meso-CF_3 BODIPY-derivative	618	636	Image mitochondrial viscosity in living cells	Intracellular viscosity	41
FB	450	588	Aβ aggregates detection		42
TPNDPA-C15	510	537/650	Viscous-dependent fluorescence to probe membrane dynamics		43
HAPH-1	410	470/580	Viscosity detection in living cells		44
CSP	460	672	Monitor mitochondrial viscosity changes		45
ATV-PY	386	498	Visualization of $ONOO^-$ and reduction of drug-induced hepatotoxicity	Intracellular ROS	47
ATV-PPB	450	651			
TPE-BOH	350/400	510/625	Ratiometric imaging of $ONOO^-$ fluctuation in mitochondria		48
CTPA	410/460	456/605	Detect endogenous and exogenous ClO^-		38
PNRFN	305/553	466/574	Lysosomal hypochlorous acid (HClO) tracking in living cells		49
PEG-*b*-P(DEAEAN-*co*-TPMA)	425	570	Hypoxia-triggered self-assembly fluorescent probe for tumor imaging	Intracellular hypoxia	50
TPE-2E *N*-oxide	313	460	*In vitro* hypoxia imaging		51
PEG-azo-PS4	418	642	Hypoxia-mediated tumor imaging and photodynamic therapy		52
TPA-BN TPA-Azo	500	650	Hypoxic tumor detection and fluorescence imaging		53
TBT/TBTO	450	592	Photo-acoustic imaging of hypoxic microenvironment		54
TPE-PBP	405	500/631	*In vitro* quantification of thiol	Intracellular biothiol	56
BQM-OH BQM-NBD	450	560	Imaging of Cys in living cells		57
TPEPY-S-Fc	430	620	Image-guided photodynamic therapy of cancer cells		58
TPE-NBD-D	353	480	Detect intracellular hydrogen sulfide		59
TPETF-NQ-cRGD	405	650	Imaging cancer cells with overexpressed $\alpha_v\beta_3$ and ablation through ROS		60
TD-Gal_6 TD-Glc_6 TD-Fuc_6	420	625	Fluorescence sensing and imaging of glycosidase activity in cells	Intracellular enzyme activity	61
QM-βgal	434	560	Tracking of β-galactosidase		62
QM-HSP-CPP	447	590	Monitor over expressed enzyme Cathepsin E (CTSE)		63
TPE-pepK TPE-pepQ	304 303	460	*In situ* imaging and real-time monitoring of intracellular tissue transglutaminase (TG2)		64
TCFPB-AChE	575	634	Real-time imaging of acetylcholinesterase (AChE) activity *in vivo*		65
DQM-SULF	430	541	Detect endogenous sulfatase in tumor cells		66

real-time and reversible monitoring of organelles accompanied by an intracellular pH change. Jia *et al.* designed an AIE probe with a large stokes shift to detect intracellular pH changes.[24] The reported probe, TPE-DCP, displayed fluorescence

Table 2 Summary of AIE probes for tracking and visualizing intracellular processes

AIEgen	Excitation (nm)	Emission (nm)	Feature(s)	Application	Ref.
TPE-4EP+	392	615	Self-reporter to induce and monitor the apoptosis process	Apoptosis	67
Berberine (BBR)	431	535	Natural AIE theranostic probe for monitoring apoptosis		68
TVQE	540	680	Monitor cell conditions by hydrolysis of intracellular esterase		69
CP1-ctrl	308	476	Caspase responsive fluorescence-magnetic probe for monitoring cell apoptosis		70
TPAP-C5-yne	420	600	Analyze motion of single mitochondrion in live primary hippocampal neurons and long-term tracking of mitochondria for up to 7 days in live neurons	Mitochondrial movement and mitophagy	71
CSP	475	678	*In situ* real-time tracking of mitochondrial membrane potential variations		72
CS-Py-BC	475	686	Monitor viscosity variation during mitophagy		73
TPA-Py	500	680	Viscosity-dependent mitophagy monitoring		74
TTVPHE	482	592	Monitor mitochondrial damaging process		75
Ag@AIE nanocarrier	480	640	Visualizing gene delivery and cancer cell inhibition	Drug and gene delivery	76
Py-TPE/siRNA@PMP	393	600	Real-time intracellular tracking of gene delivery and long-term tumor tissue imaging		77
TPE-DEVD-RGD	320	480	Real-time visualization of drug delivery and release for cancer cell apoptotic therapy		78
PEG-Pep-TPE/DOX nanoparticle	350	490	Real-time drug release monitoring		79
MeTPAE	424	632	Bind to nucleic acid for long-term monitoring of the nucleus division process in cell viscosity in living cells	Nucleus division monitoring	80
TPEPy-D-Ala	390	700	Turn-on imaging of intracellular Gram-positive bacteria through peptidoglycan metabolism	Intracellular bacteria monitoring	81
TPACN-D-Ala	450	610	Metabolic labeling of intracellular Gram-positive bacteria and *in vivo* ablation		82
TPEPy-Ala	374	528	Light-up and identify intracellular Gram-positive bacteria through metabolic incorporation in the peptidoglycan		83
TPAPy-Kdo	447	595	Light-up and visualize intracellular Gram-negative bacteria through metabolic incorporation in the lipopolysaccharide		83
TTVP	480	704	Tracing of bacterial phagocytosis process		84
TPEPy-Et	380	650	Detect macrophage-engulfed bacteria		85
TBTCP	514	723	Monitor phagocytosis by observing plasma membrane dynamics	Cellular response to bacteria entry	86
PyTPE-CRP	400	610	Monitor phagosome formation of macrophages with bacterial infection		87
DTF–FFP nanoparticles	480	650	Visualize and ablate bacteria in phagocytes		88

enhancement in an acidic environment and a dramatic decrease in fluorescence in a basic environment. Intracellular pH detection from 4.5–8.5 by fluorescence enhancement was achieved in HepG2 cells where TPE-DCP displayed gradual red emission enhancement with the strongest signal at pH 4.5. Wang *et al.* reported a reversible AIE probe for bioimaging of pH levels in cells based on a lactone hydrolysis strategy.[25] The active lactone moiety in the TCC probe undergoes hydrolysis under weak basic conditions. TCC displays green emission in HeLa cells of pH 6, and a gradually reduced green emission could be observed when increasing the pH value. At pH 9, the green emission is almost unnoticeable, with a strong red emission appearing, suggesting the occurrence of the hydrolysis reaction, yielding a water-soluble TCHC product with red-shifted emission.

Cellular temperature

Temperature is a critical physiological factor that drives the biochemical reactions and dynamics in a living cell. Cells and enzymes respond to temperature fluctuations quickly, and temperature can affect a wide range of cellular functions, such as the rate of protein folding, cellular respiration, metabolism, *etc.* In addition, cellular disorders are also found to be accompanied by temperature increases.[26,27] The use of AIE probes could dynamically monitor the intracellular temperature to help further study biological activities. De *et al.* reported a

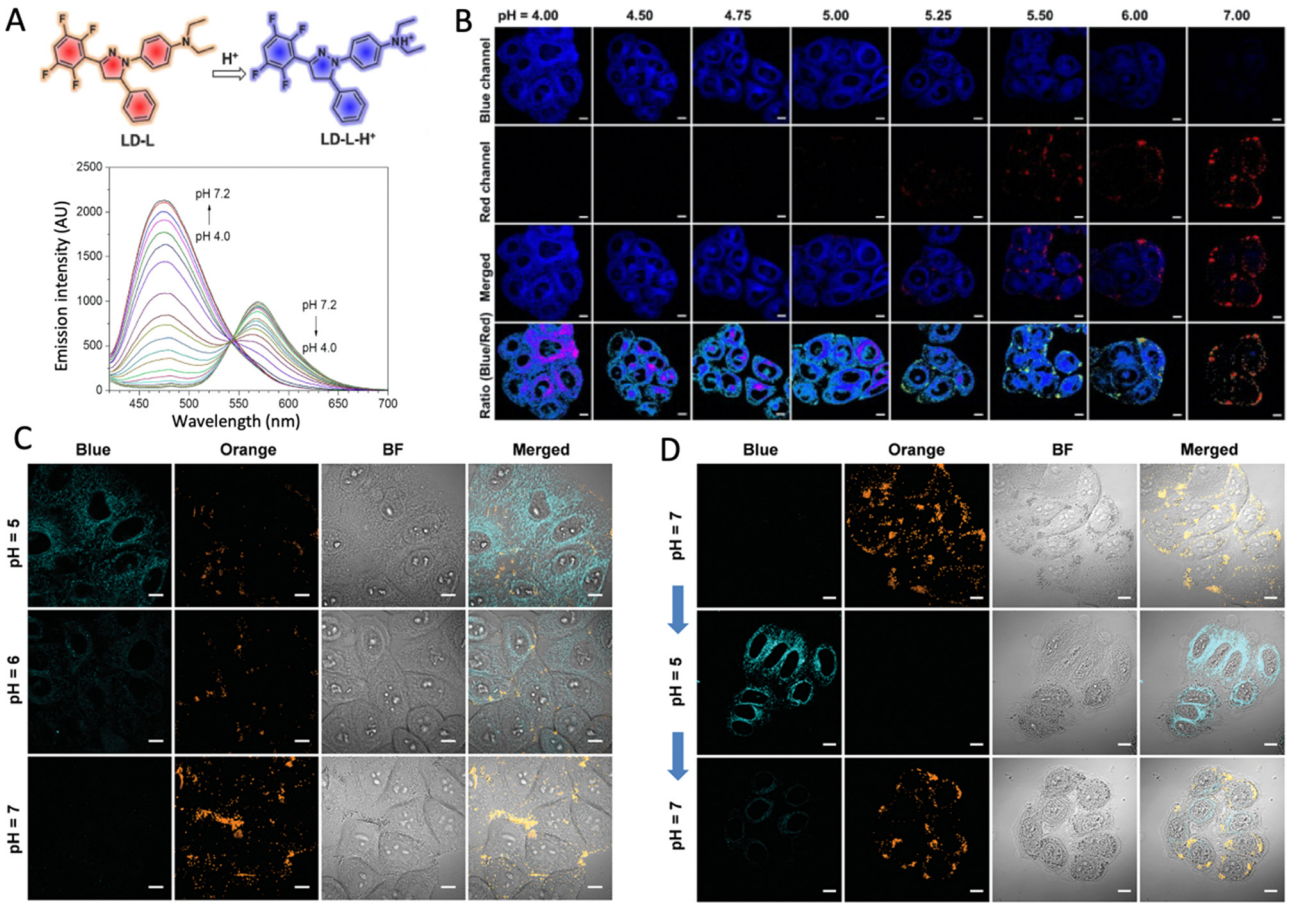

Fig. 1 Ratiometric probing and imaging of intracellular pH level. (A) Chemical structure of LD-L and emission spectra of LD-L with different pH values (4.0–7.2). (B) Confocal images of HeLa cells stained with LD-L at different pH conditions. Scale bar: 10 μm. Reproduced with permission from ref. 20. Copyright 2022 Elsevier. (C) Confocal images of HeLa cells stained by Pyr-5 at different pH values. Scale bar: 10 μm. (D) Confocal images of HeLa cells stained by Pyr-5 with *in situ* adjusting of the intracellular pH value. Scale bar: 10 μm. Reproduced with permission from ref. 23. Copyright 2019 Royal Society of Chemistry.

non-conjugated poly(*N*-vinylcaprolactam) (PNVCL) as an AIE-active fluorescent thermometer for intracellular temperature imaging.[28] PNVCL displayed not only AIE properties and cluster-oluminescence but also excitation-dependent emission due to various excited states. As PNVCL has been previously reported to exhibit a temperature-dependent phase transition, its thermal response was further investigated by incubating in MCF-7 cells under different temperatures (Fig. 2A). After incubation at 25 °C and 35 °C, green and red emissions could not be observed with weak blue fluorescence. At 38 °C, a temperature-induced fluorescence enhancement inside the cell could be observed in blue, green, and red emission channels (Fig. 2B). The lowest critical solution temperature (LCST) of PNVCL was found to be 37.5 °C, evidenced by an abrupt decrease in the solution transmittance. It is believed that the rupturing of hydrogen bonds occurs at higher temperatures. PNVCL displayed no emission when below the LCST. A strong blue fluorescence could be observed when the temperature reached above the LCST due to the heat-induced polymer conformational change leading to an AIE effect (Fig. 2C). Similarly, PNVCL undergoes a temperature-dependent turn-on when incubated inside cells. The fluorescence intensity showed approximately 50 and 29-fold increments when the temperature reached above the LCST (Fig. 2D). Huang *et al.* reported a thermoprobe based on phosphorescent probes that could detect intracellular temperature from 25 to 35 °C with enhanced emission.[29] Interestingly, the variation in the phosphorescence intensity was observed in different locations of HepG2 cells, suggesting potential utilization for intracellular temperature distribution imaging. Zhu *et al.* developed a thermoresponsive probe for cell imaging. The probe LCAPU-TPE is made up of TPE-acid conjugated to polymer chain ends and displayed a linear decrease in fluorescence with increasing temperature.[30] The temperature effect of LCAPU-TPE was studied in A375, L929, and HepG2 cells from 31 to 45 °C. With increasing temperature, the green fluorescence became weaker up to 45 °C. After cellular uptake, the TPE unit is bound to the CA moiety producing strong fluorescence and undergoes rotation relaxation with increasing temperature. Tian *et al.* designed a ratiometric fluorescent thermometer for sensing intracellular temperature by fabricating nanoparticles with a thermosensitive AIEgen and Rhodamine 110 using the F127

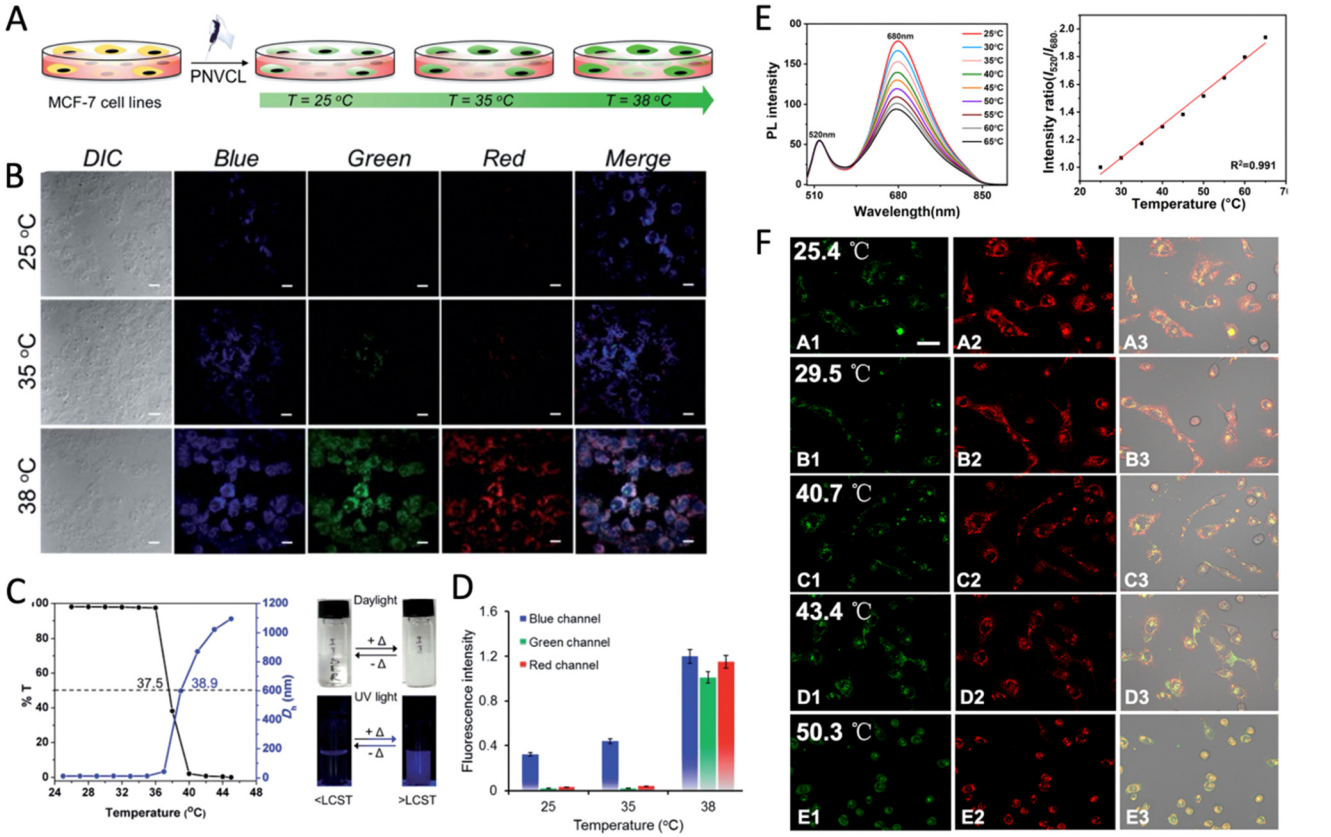

Fig. 2 AIEgens for performing temperature-dependent intracellular imaging. (A) Schematic representation of MCF-7 cells co-cultured with auto fluorescent PNVCL at different temperatures. (B) Confocal images of MCF-7 cells labelled with PNVCL at different temperatures for 24 h. Scale bars = 10 μm. (C) Variation of %*T* and D_h of PNVCL solution as a function of temperature and photographs of PNVCL solution under daylight and UV irradiation at 365 nm below and above the LCST. (D) Fluorescence intensity ratio of PNVCL at different color channels over 4′,6-diamidino-2-phenylindole (DAPI) fluorescence signal in MCF-7 cells. Reproduced with permission from ref. 28. Copyright 2020 Royal Society of Chemistry. (E) PL spectra of TRF NPs with increasing temperature from 25 to 65 °C. PL intensity ratio *versus* temperature curves of TRF NPs. (F) Confocal images of TRF NP-treated Hep-G2 cells at different temperatures. Scale bar = 50 μm. Reproduced with permission from ref. 31. Copyright 2020 American Chemical Society.

matrix.[31] The resultant TRF NPs showed dual emission ratiometrically concerning temperature changes. The emission peak at 680 nm significantly reduced with increased temperature, whereas the emission at 520 nm remained unchanged. TRF NPs in aqueous solution displayed an excellent sensitivity of 2.37% in a broad temperature range of 25 to 65 °C with reversibility up to 10 cycles (Fig. 2E). Dynamic intracellular temperature monitoring revealed that TRF NPs displayed strong red and green emissions at 25.4 °C. As the temperature rose, the green emission intensity remained relatively the same while the red emission intensity gradually weakened (Fig. 2F).

Cellular polarity

Cell polarity is important as it plays a critical role in cellular development and function. For instance, the apical and basal parts of epithelial cells create a barrier against pathogen invasion. Another example would be the front-to-back polarity that allows cells to adhere and detach during cell migration.[32] Cell polarity also creates a distinct shape and morphology of cells. Moreover, cell polarity could also indicate disease or cancer progression. The loss of cell polarity is a hallmark of cancer and can also be associated with abnormal cell accumulation.[33] Due to the polarity difference within the cellular structure, monitoring and differentiating the polarity-different cellular compartment could be realized by fluorescent probes exhibiting both AIE and twisted intramolecular charge transfer (TICT) features. AIE and TICT probes could undergo emission shift and color change depending on the degree of intracellular twisting and charge transfer due to the polarity difference within the cellular compartments.

Zhu *et al.* reported a polarity-sensitive fluorescent probe named TICT-lipid that can reflect the degree of packing within the bacterial membrane by emission change.[34] Due to the intrinsic donor-acceptor effect, TICT-lipid displayed an emission redshift along with increasing polarity. As illustrated in Fig. 3A, TICT-lipid displayed a blue-shifted emission changing from red to yellow in PBS to *E. coli* and *MRSA*, indicating the different TICT interactions in bacteria. TICT-lipid was found to localize in the densely packed lipids of Gram-positive bacteria, resulting in twisting, which was reflected by a more pronounced emission blue shift. The loosely packed lipids of the Gram-negative outer membrane result in intercalation, causing

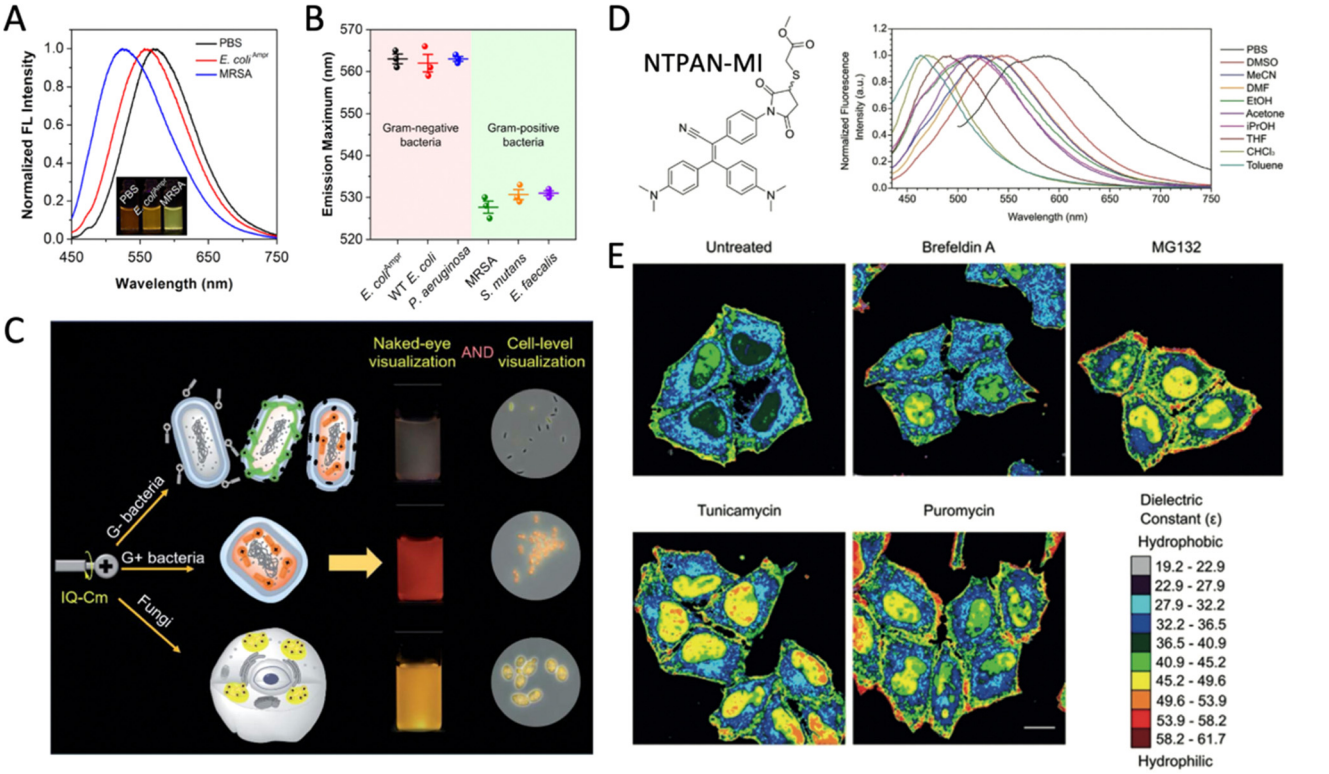

Fig. 3 AIE-TICT based intracellular polarity sensitive probes. (A) Normalized emission spectra of TICT-lipid postincubation with PBS, *E. coli*^{Ampr}, and MRSA. Inset: A photograph taken under a 365 nm UV lamp. (B) Emission maximum of TICT-lipid postincubation with six different bacteria. Reproduced with permission from ref. 34. Copyright 2022 American Chemical Society. (C) Schematic illustration of IQ-Cm for visual classification of various pathogens. Reproduced with permission from ref. 35. Copyright 2020 Royal Society of Chemistry. (D) Chemical structure of NTPAN-MI. Normalized fluorescence spectra in solvents with different polarity. (E) Representative images of intracellular dielectric constant distribution of normal cells and stressed cells. The cells were stained by NTPAN-MI. Scale bar: 20 μm. Reproduced with permission from ref. 39. Copyright 2019 Wiley-VCH.

only a slight blue shift. The fluorescence response could enable monitoring the localization of the probe within the bacteria as well as differentiating different bacterium types (Fig. 3B). Tang's *et al.* also reported a microenvironment-sensitive probe for bacterial differentiation.[35] Due to the intrinsic structural difference of pathogens, IQ-Cm exhibiting AIE and TICT properties showed emission color change (Fig. 3C). The prominent AIE and TICT effect of IQ-Cm allowed for an obvious and naked-eye observable fluorescence response. Distinguishable emission colors could be easily observed after incubation with different pathogens, with a soft pink color for Gram-negative bacteria, orange-red fluorescence for Gram-positive bacteria, and strong yellow for fungi. The difference in emission suggests different binding affinities and localization of IQ-Cm inside the pathogen. IQ-Cm was found to remain in the cell membrane of Gram-negative bacteria, while IQ-Cm can penetrate and localize in the cytoplasm of Gram-positive bacteria and fungi, generating a red-shifted emission as it has been reported to be a more water-like and polar environment. Beside utilization in bacterial studies, Lin *et al.* designed a polarity-sensitive probe for monitoring cancer cells.[36] It has been reported that the amount of lipid droplets in cancer cells shows reduced polarity. The reported TR-1 probe enabled the monitoring of lipid droplets in 4T1 and HepG2 cancer cells. Because of the TICT effect of TR-1, a stronger and blue-shifted emission could be observed in a lower polarity environment *versus* a weak and red-shifted emission in a higher polarity environment. As a result, TR-1 could dynamically monitor and differentiate cancer cell progression by the environmental polarity difference and fluorescence response. Another study by Lin *et al.* demonstrated intracellular polarity mapping of lipid droplets. The reported BF_2 chelated AIE probe (LDs-BCA) could monitor cell polarity in real time, particularly the dynamic metabolic response of lipid droplets in a living mouse.[37] Based on a similar TICT design strategy, LDs-BCA displayed a significant fluorescence signal in the gastric region of the mouse with obesity compared to a normal mouse. The accumulation of gastric fat in mice with obesity led to a reduced polarity resulting in a strong fluorescence signal that was observable for up to 12 h, while normal mice showed negligible signal due to the regular polarity environment. Yan *et al.* similarly designed a fluorescent probe (CTPA) for detecting polarity in living cells by displaying a red-shifted emission.[38] In response to the polarity fluctuation in HeLa and NIH-3T3 cells, CTPA displayed enhanced fluorescence intensity and emission redshift. Hong *et al.* presented a NTPAN-MI probe for quantifying subcellular polarity changes.[39]

Fig. 3D depicts thiol-bound NTPAN-MI with a push-pull effect resulting in a solvatochromism property. The emission spectra displayed a strong red shift with the increase of solvent polarity, from 465 nm in toluene to 586 in PBS solution. Due to the presence of the thiol group, NTPAN-MI showed excellent cysteine (Cys) reactivity and detection of unfolded protein could be observed by enhanced fluorescence upon the addition of drugs that interfere with protein synthesis. Furthermore, NTPAN-MI was confirmed to interact with protein rather than DNA, evident by the localization within the endoplasmic reticulum (ER). Under stress conditions, protein condensation also occurs in the nucleus. However, the co-localization experiment verified the protein-specific interaction of NTPAN-MI. The excellent advantage of the solvatochromism effect and cellular distribution enabled NTPAN-MI for the polarity study of bound proteins in cells. NTPAN-MI revealed the dielectric constant of the labeled proteins in different cellular compartments (Fig. 3E). Unfolded proteins in the ER exhibit a lower dielectric constant because of the more hydrophobic environment, while a more hydrophilic environment in the nucleus contributes to a higher dielectric constant. The solvatochromism property NTPAN-MI not only enables subcellular polarity measurement but also reveals intracellular communication, which is critical for numerous biological processes like protein synthesis and stress management.

Intracellular viscosity

Intracellular viscosity is a key parameter affecting diffusion in the biological process, such as cellular reaction rates, cellular signaling, transportation of molecules and proteins, *etc.* The viscosity in the cell has been reported to range from 1–400 cP depending on the subcellular compartment. Abnormal intracellular viscosity can be associated with cellular malfunctioning as well as diseases.[40] Given the vital role viscosity plays in maintaining cellular function, visualizing real-time changes in cellular viscosity is highly desired. Yan *et al.* designed an AIE active BODIPY-derivative that showed a sensitive response to cell viscosity change (Fig. 4A).[41] The introduction of a CF_3 at the *meso* position of the core showed excellent AIE properties and red-shifted emission. The introduction of a cationic group enabled mitochondria targeting selectivity. It was found that the BODIPY-derivative presented aggregated micelles in water and was weakly emissive. Upon the addition of glycerol, substantial fluorescence enhancement was observed, attributed to the restriction of rotation of the *meso*-CF_3 group. Given the cationic group, the BODIPY-derivative could target the mitochondria, and upon viscosity changes, fluorescence enhancement could be observed. Human neuroblastoma cells were used to study the monitoring of viscosity change in cells. Fig. 4B shows that only a weak red emission could be observed after treating low-viscosity SH-SY5Y cells with BODIPY derivatives. The treatment of lipopolysaccharide to increase cellular viscosity led to strong fluorescence which can be explained by the LPS-induced increase of viscosity leading to a restriction of the *meso*-CF_3 group, thus generating strong fluorescence. Yan *et al.* developed another AIE probe for visualizing viscosity changes in cells by fluorescence response.[42] The reported FB probe showed a viscosity fluorescence response in SH-SY5Y

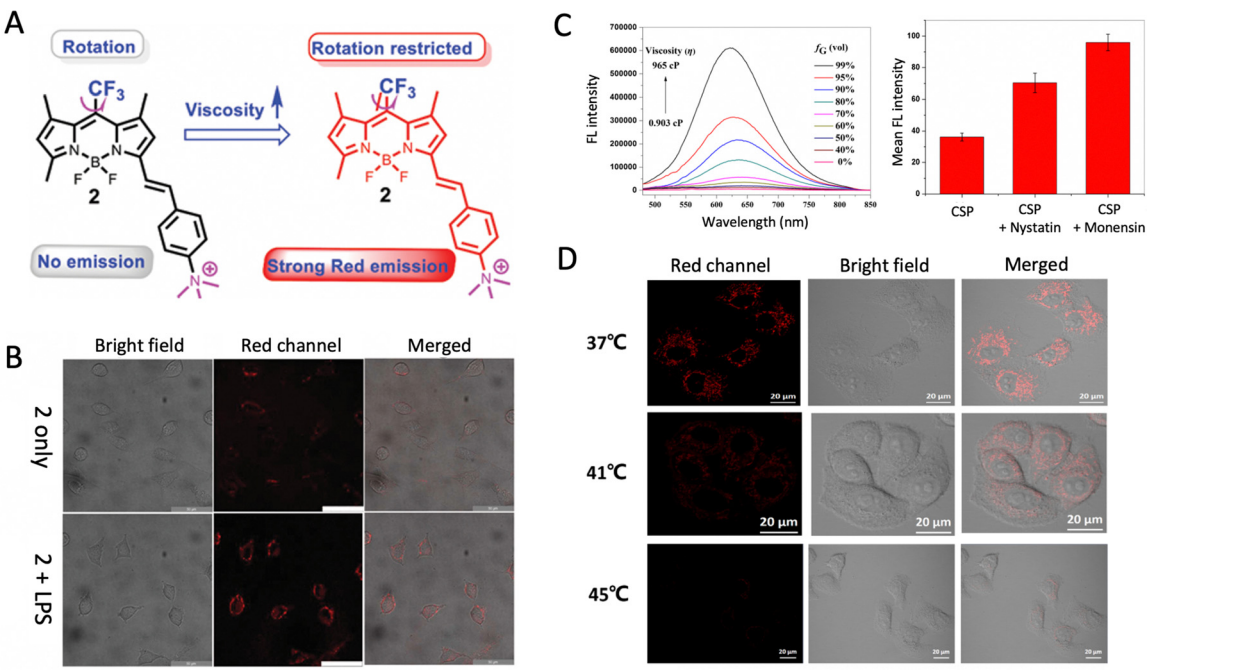

Fig. 4 AIEgens as viscosity monitoring probes in living cells. (A) Chemical structure and mechanism of 2 responding to mitochondrial viscosity changes. (B) Confocal images of SH-SY5Y cells pretreated with DMEM or LPS, followed by incubation with 2. Reproduced with permission from ref. 41. Copyright 2022 Royal Society of Chemistry. (C) Emission changes of CSP in different water/glycerol mixtures. Mean fluorescence intensities before and after treatment with nystatin or monensin. (C) Confocal images of HeLa cells pretreated with nystatin or monensin, and then incubated with CSP. Reproduced with permission from ref. 45. Copyright 2021 Springer.

cells. FB showed no fluorescence signal in untreated SH-SY5Y cells. However, a strong fluorescence could be visualized after treating SH-SY5Y cells with monensin and nystatin, which causes an increase in the cytoplasmic viscosity. Tong *et al.* reported a viscosity-sensitive AIE probe for a lipid order imagery study.[43] The AIE membrane-specific probe called TPNDPA-C15 emits red fluorescence upon restriction of intramolecular motion in normal viscous HeLa cell membranes and displays a yellow emission in the loosely packed membrane. These different fluorescence responses could reflect the membrane lipid packing order and visualization of numerous cellular processes encompassing membrane dynamics. Zhu *et al.* reported an AIEgen (HAPH-1) based on styrlquinoline for viscosity detection in live cells through two-photon microscopy.[44] HAPH-1 initially showed weak yellow emission after incubating with HeLa cells. It has been previously reported that decreased cellular temperature is associated with increased cellular viscosity. When the incubation temperature was gradually decreased, an enhanced yellow emission was observed due to the increase in intracellular viscosity. Moreover, HeLa cells treated with nystatin as an ionophore to induce swelling, which leads to dysregulation of viscosity, displayed significant yellow emission enhancement. Dong *et al.* presented an AIE CSP probe sensitive to viscosity changes.[45] The cationic pyridinium group in CSP allowed for selective mitochondria targeting ability. CSP displayed fluorescence enhancement upon a viscosity increase. When CSP is incubated with ionophore pre-treated HeLa cells, the fluorescence intensity is significantly stronger than control HeLa cells due to a stronger mitochondrial viscosity (Fig. 4C). The dynamic changes in mitochondrial viscosity during heat stroke were monitored. As depicted in Fig. 4D, increasing the cellular temperature from 37 to 45 °C displayed a weakened fluorescence trend due to reduced viscosity in higher cellular temperatures. CSP exhibited excellent mitochondrial selectivity, and its viscosity-sensitive showed great potential for monitoring mitochondrial dynamics and heat-stress injury.

Intracellular ROS and hypoxia

Reactive oxygen species (ROS) are cell signaling molecules for biological processes. However, ROS generation also provokes cellular damage and disrupts normal physiology. Besides, ROS dysregulation is also found to be associated with diseases.[46] Many AIE probes were reported to exhibit a turn-on phenomenon for ROS and hypoxia conditions. Due to their excellent photostability, AIE probes also enable monitoring of the dynamic intracellular ROS and hypoxia conditions. Tang *et al.* reported a ratiometric AIE probe ATV-PPB for monitoring the peroxynitrite level in liver cells (Fig. 5A).[47] ATV-PPB localizes in the mitochondria in the absence of peroxynitrite, and green fluorescence could be observed in the lipid droplets when peroxynitrite is formed. As displayed in Fig. 5B, ATV-PPB initially showed a red signal in the absence of acetaminophen. Excessive acetaminophen is reported to induce the formation of peroxynitrite, and green fluorescence emerged at 12 h and continuously intensified. As the time was prolonged, acetaminophen induced the formation of peroxynitrite, which reacted with ATV-PPB to yield green emissive ATV-Py. Zhang *et al.* also reported a ratiometric TPE-BOH probe with an AIE property for imaging the fluctuation of peroxynitrite in mitochondria.[48] The boronate act as the receptor unit, in which the cationic pyridinium was transformed into neutral pyridine in the presence of peroxynitrite. An obvious ratiometric change could be observed with enhanced green and reduced red fluorescence in RAW264.7 cells. Yan *et al.* designed a fluorescent probe CTPA for detecting hypochlorite in living cells.[38] CTPA was successfully utilized for detecting endogenous and exogenous hypochlorite in HeLa and HIN-3T3 cells. With the concentrations of hypochlorite increasing, the fluorescence intensity of cells gradually increased, suggesting that CTPA could dynamically image exogenous and endogenous hypochlorite levels. Zhang *et al.* developed a ratiometric fluorescent nanoparticle (PNRFN) for sensing endogenous hypochlorite in lysosomes.[49] Upon treating the HeLa cells with PNRFN, bright blue and red emission signals could be observed in the lysosomes. In the presence of hypochlorite concentration in HeLa cells, the red fluorescence is gradually weakened, with the blue fluorescence remaining unchanged, demonstrating its ratiometric response toward hypochlorite.

Apart from abnormal intracellular ROS levels, low oxygen levels also lead to cellular malfunction and cell death. Hypoxia is a common condition in which the oxygen demand exceeds the oxygen supply leading to hypoxic stress and cell death. He *et al.* designed a hypoxia-triggered *in situ* self-assembly fluorescent probe for imaging by incorporating azobenzene moiety and long-wavelength AIEgen.[50] The AIEgen containing polymer showed negligible fluorescence due to the quenching effect and good water solubility (Fig. 5C). Under hypoxia conditions, the reduction of azobenzene transformed cationic quaternary ammonium to anionic carboxylate leading to the self-assembly of nanoparticles inside living cells with fluorescence. Fig. 5D shows that HeLa cells under normoxic conditions showed dark and negligible fluorescence. Gradually decreasing the oxygen supply led to increased fluorescence intensity, confirming the nanoparticle's ability for dynamic monitoring of oxygen levels in living cells. Tang *et al.* designed a hypoxia-responsive probe for *in vitro* hypoxia imaging. The reported TPE-2E *N*-oxide probe has two *N*-oxide groups, which will be cleaved by cellular reductase overexpressed under hypoxic conditions, producing turn-on hypoxia imaging.[51] A PEGlated AIE probe for hypoxia imaging was developed by Li *et al.*[52] The reported AIE probe has a hypoxia-sensitive azo group with PEG chains. The PEG chains result in the water solubility of the reported probe, and upon reductase cleavage, the remaining AIE probe will form aggregates in an aqueous medium leading to fluorescence. Li *et al.* constructed another hypoxia-responsive probe TPA-Azo that can image lipid droplets and lysosomes following a similar approach.[53] The overexpression of azoreductase can reduce TPA-Azo in hypoxia tumors to generate fluorescence. Tang *et al.* designed a hypoxia-activated probe for NIR fluorescence and photoacoustic (PA)

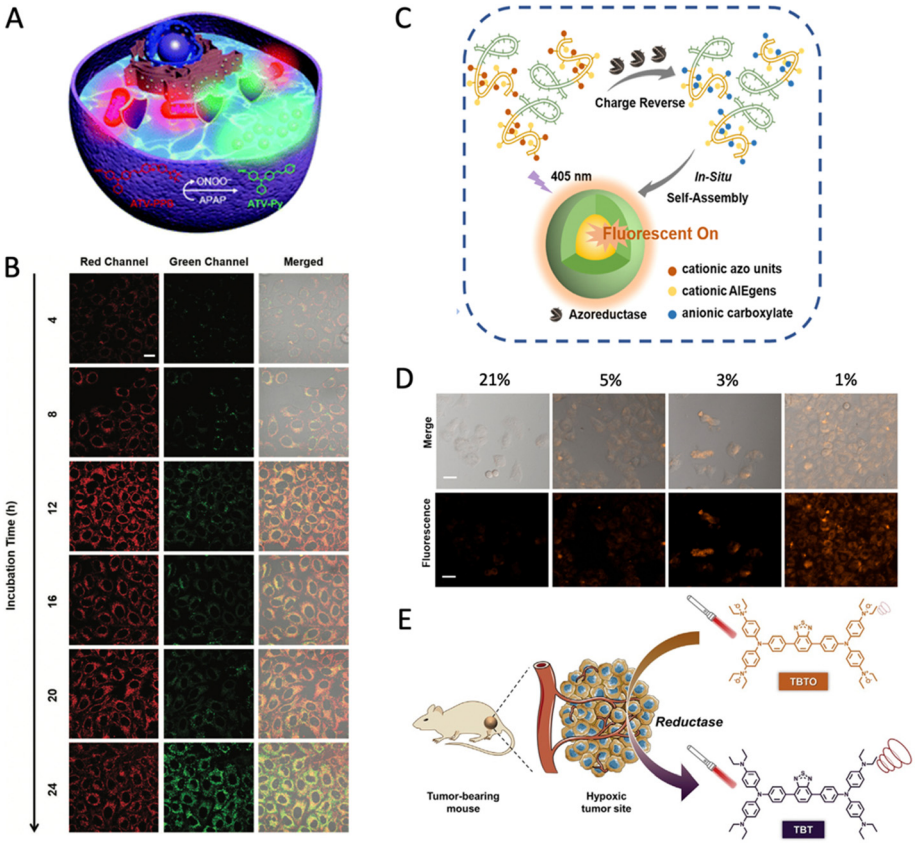

Fig. 5 AIE probes for intracellular sensing and imaging of ROS and hypoxia conditions. (A) Schematic illustration of $ONOO^-$ reduction of ATV-PPB inside mitochondria. (B) Time tracking of HepG2 cells stained with ATV-PPB and APAP. Scale bar: 20 μm. Reproduced with permission from ref. 47. Copyright 2022 Royal Society of Chemistry. (C) Schematic illustration of azobenzene reduction, charge reverse, *in situ* self-assembly, and fluorescence turn-on process. (D) Confocal images of adherent HeLa cells incubated with PEG-*b*-P(DEAEAEN-*co*-TPMA) under normoxic (21% v/v O_2) and different hypoxic (5%, 3%, 1% v/v O_2) conditions. Scale bars: 50 μm. Reproduced with permission from ref. 51. Copyright 2021 American Chemical Society. (E) Schematic diagram of hypoxia-activated probe for fluorescence and photoacoustic tumor imaging. Reproduced with permission from ref. 54. Copyright 2021 CellPress.

imaging (Fig. 5E).[54] The hypoxia-activated probe TBTO features four *N*-oxide groups, which could undergo bio-reduction in a hypoxic environment to produce TBT with a donor-acceptor-donor structure displaying NIR emission and PA signal. The PA signal could still be detected after 3 days of injection, suggesting the utility for long-term tracking and monitoring.

Intracellular biothiol levels

Biothiol participates in many intracellular reactions against oxidative stress. For example, glutathione (GSH) is an antioxidant that defend against free radicals and sustains intracellular redox homeostasis.[55] However, abnormal biothiol levels are directly correlated to many diseases. Therefore, monitoring the intracellular biothiol is vital in understanding pathophysiological conditions as well as providing important insights into disease diagnosis. Tang *et al.* reported a ratiometric AIE probe for mitochondrial thiol detection.[56] The *para*-dinitrophenoxy benzylpyridinium moiety was introduced as an electron-accepting unit to redshift the emission and act as a mitochondrial targeting group (Fig. 6A). The reported TPE-PBP probe showed red fluorescence, and the addition of thiol resulted in blue-shifted emission due to cleavage of the dinitrophenyl ether bond producing a less conjugated AIEgen (Fig. 6B). It is believed that the green fluorescence originated from TPE-Py, which is produced by the reaction between TPE-PBP and mitochondrial thiol, and the red fluorescence originated from TPE-PBP itself (Fig. 6C). When the biothiol level in the HeLa cells is increased, a reduced green fluorescence signal could be observed, accompanied by an enhanced red fluorescence (Fig. 6D). Wang *et al.* presented a BQM-OH probe containing 7-nitro-1,2,3-benzoxadiazole (NBD) as the recognition moiety for Cys and homocysteine (Hcy).[57] The selectivity of BQM-OH is believed to be attributed to the sulfhydryl group of Cys and Hcy, and the resulting intermediate undergoes rearrangement to obtain NBD-Cys and NBD-Hcy. Kim *et al.* presented a simple design of TPEPY-S-Fc linked by a disulfide bond for GSH cleavage.[58] The resultant TPEPY-SH is released to display enhanced fluorescence in CT-26 cells. Maiti *et al.* designed a TPE-NBD-D probe by appending with a 4-chloro-7-nitrobenzofurazan (NBD) and disulfide-linked donor.[59] The disulfide-linked donor is cleaved off by esterase, and the counterpart will generate a turn-on fluorescence after releasing

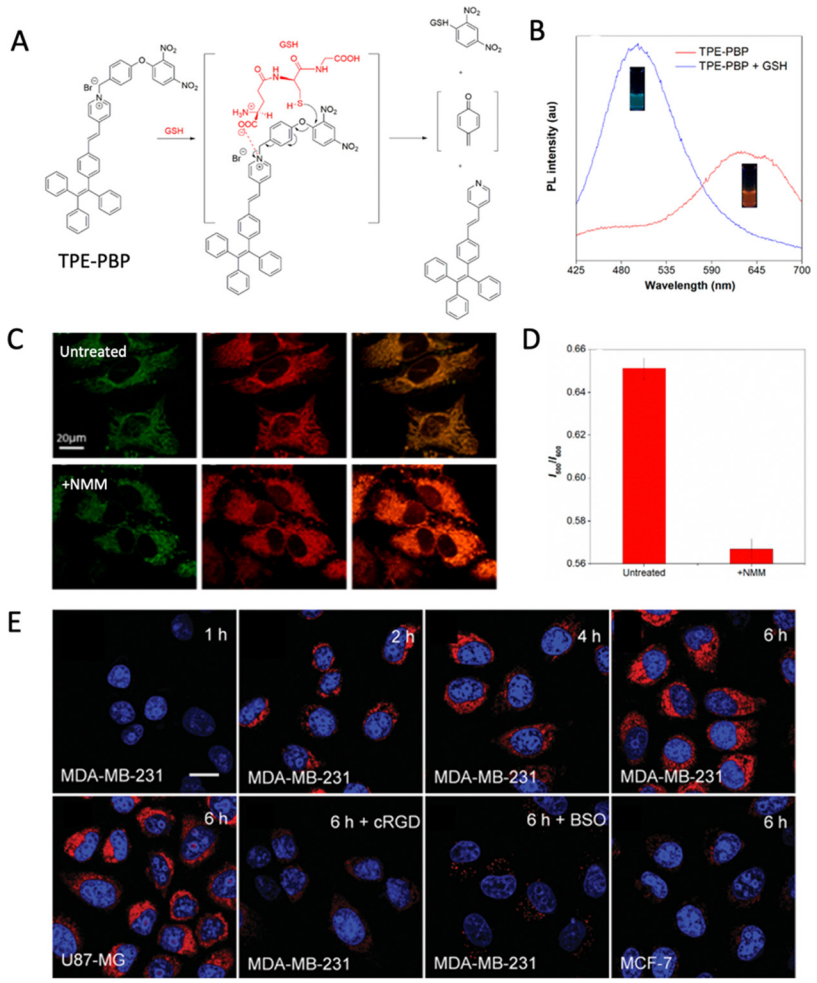

Fig. 6 Tracing of intracellular biothiols by AIEgens. (A) Proposed mechanism for selective reaction of TPE-PBP toward biothiols. (B) PL spectra of TPE-PBP before and after GSH treatment. Inset photographs of TPE-PBP solutions before and after addition of GSH taken under UV light at 365 nm. (C) Intracellular biothiol detection using TPE-PBP in untreated HeLa cells and NMM treated HeLa cells. Scale bar = 20 μm. (D) Relative PL intensity of NMM and TPE-PBP treated HeLa cells. Error bars are ± relative standard deviations, n = 3. Reproduced with permission from ref. 56. Copyright 2019 American Chemical Society. (E) Confocal images of various cell lines pre-incubated with cRGD or BSO and further incubated with AIE probe for different amounts of time. Scale bar = 20 μm. Reproduced with permission from ref. 60. Copyright 2016 Royal Society of Chemistry.

NBD ligand in the biothiols environment. The probe enabled intracellular hydrogen sulfide detection in SH-SY5Y cells by a turn-on response. The probe was also utilized in an *in vivo* mice model to study further the involvement of hydrogen sulfide-releasing molecules in managing Alzheimer's disease. Liu *et al.* developed a probe with a quencher moiety that can be restored after receptor-mediated endocytosis and intracellular GSH activation.[60] The probe was incubated with cancer cells of U87-MG and MDA-MB-231. As cancer cells show higher GSH concentrations, it is anticipated that the probe could accumulate more in cancer cells through receptor-mediated endocytosis and further undergo GSH-induced release of quencher moieties leading to turn-on fluorescence. As shown in Fig. 6E, the red fluorescence in cancer cells increased gradually with incubation time, while no signal could be observed in normal cells. Thus, the probe enabled dynamic monitoring of intracellular GSH levels by endocytosis first and GSH activation.

Intracellular enzyme activity

Enzymes inside cells catalyze millions of metabolic reactions, including photosynthesis and cellular respiration. Dysfunctional enzymatic activity is believed to be an underlying cause of numerous diseases. Intracellular enzymes may be present in either cytoplasmic fluid or bound to organelles. With the help of AIE probes, fluorescence imaging of the enzyme activity could be achieved. Vidal *et al.* demonstrated intracellular sensing of various glycosidases using AIE-based glycoclusters (Fig. 7A).[61] Introducing six copies of monosaccharides through azide-click reaction to the dendritic linkages on TPE-DCM enabled its selectivity towards a diverse range of glycosidases, including β-D-galactosidase, β-D-glucosidase, and α-L-fucosidase. The reported probe enabled imaging of endogenous glycosidase activities in cells and long-term imaging of glycosidase-activated cells. In Fig. 7B, weak fluorescence was initially observed after incubation of TD-Gal_6 with SKOV-3 cells

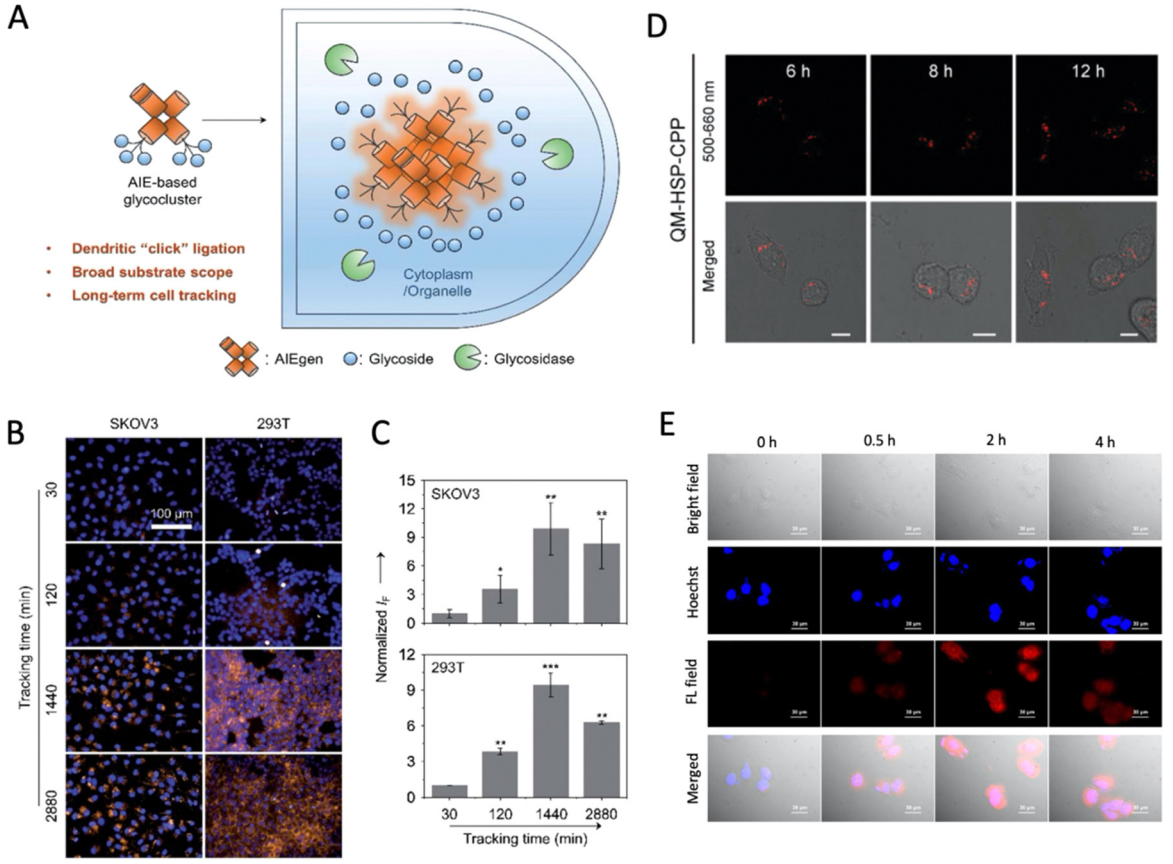

Fig. 7 AIE probes to track intracellular enzyme activity. (A) Schematic illustration of AIE-based glycoclusters for the detection of a wider range of glycosidases that enable long-term intracellular glycosidase-activated fluorescence tracking. (B) Fluorescence imaging and SKOV-3 cells and 293T cells incubated with TD-Gal_6, TD-Fuc_6 and Hoechst 33342. Reproduced with permission from ref. 61. Copyright 2022 Royal Society of Chemistry. (C) Quantification of SKOV-3 and 293T cells after incubation with TD-Gal6 and TD-Fuc6. (D) Fluorescence imaging of SW1990 cells treated with QM–HSP for different amounts of time. Scale bar = 20 μm. Reproduced with permission from ref. 63. Copyright 2022 Wiley-VCH. € Fluorescence image of H460 cells incubated with DQM-SULF at different times. Scale bar = 30 μm. Reproduced with permission from ref. 66. Copyright 2021 Elsevier.

for 30 min due to insufficient glycosylation of the intracellular glycoclusters. As the incubation time was increased, an increase in the proportion of de-glycosylated AIEgens led to enhanced fluorescence. Similarly, TD-Fuc_6 treated 293T cells showed a similar trend in fluorescence change. Both probes showed excellent fluorescence intensity enhancement that could monitor the enzymatic activity in real time, and imaging could be achieved for more than 48 h (Fig. 7C). Zhu *et al.* utilized a similar approach to develop a QM-βgal for intracellular sensing and tracking of β-galactosidase in ovarian cancer cells.[62] QM-βgal is water soluble and non-emissive in aqueous media and upon activation of β-gal, fluorescence will be restored by cleavage. Its fluorescence signal intensifies with prolonged incubation time attributed to forming more QM-OH leading to stronger fluorescence. Zhu *et al.* also designed an enzyme-activable probe of QM-HSP-CPP for monitoring the overexpressed enzyme Cathepsin E (CTSE).[63] The probe is made up of QM-COOH fluorophore, CTSE-responsive peptide, and cell penetrable peptide CPP. It was found that QM-HSP without CPP peptide aggregated on the surface of cells while introducing the CPP peptide ensures QM-HSP-CPP could enter cells. By extending the incubation time, QM-HSP-CPP will be gradually cleaved, and aggregate inside cells will show fluorescence enhancement for real-time monitoring of the CTSE activity (Fig. 7D). Liu *et al.* present a strategy for real-time monitoring of intracellular tissue transglutaminase (TG2) based on two AIE probes.[64] TPE-pepK and TPE-pepQ were prepared by click reaction between TPE-N3 and substrate pepK and pepQ. Both TPE-pepK and TPE-pepQ showed excellent water solubility. Therefore, they are non-emissive. Once internalized into cells, the presence of TG2 would cause specific crosslinking of pepK and pepQ which induced aggregation of the TPE molecule leading to a fluorescence on effect. The AIE probes could detect intracellular TG2 expression in living cells and monitor TG2 level changes in different cell types by increased fluorescence intensity. Kolemen *et al.* introduced an acetylcholinesterase (AChE) selective probe for visualizing AChE activity *in vitro* and *in vivo*. The reported TCFPB-AChE could image AChE activity in the glioblastoma cell line and living mice brains *in vivo*. Molecular docking studies suggest that TCFPB-AChE may bind to active amino acid residues of the targeting protein.[65] Hydrophobic interaction also occurs with some of

the hydrophobic amino acid residues to stabilize the small molecules. A sulfatase-activable AIE probe was developed by Wang *et al.* for tracking sulfatase. TPE-derivative with a sulfatase recognition unit self-assembled into nanoparticles which could be activated by the catalytic domain of sulfatase to afford hydrophobic DQM-OH, which shows fluorescence on and can further interact with the hydrophobic site of sulfatase to generate stronger fluorescence.[66] As cancer cells are reported to show high sulfatase activity, the probe showed a time-dependent fluorescence enhancement in H460 and A549 cells due to the increased formation of DQM-OH (Fig. 7E).

3. Tracking and monitoring of intracellular bioprocess

Apoptosis

Apoptosis is the bioprocess of programmed cell death initiated during early development to eliminate unwanted cells. In addition, apoptosis also plays an important role in preventing cancer, and it is generally found that photodynamic therapy treatments take part in apoptosis that can facilitate the anticancer effect. Therefore, apoptosis monitoring can provide an on-time indication of the therapeutic efficacy. Tang *et al.* developed AIEgen TPE-4EP , which can induce cell apoptosis by the intrinsic high ROS generation efficiency under light irradiation (Fig. 8A).[67] Moreover, this fluorescent probe can differentiate apoptotic cells from healthy cells. TPE-4EP+ also serves as a self-reporter to monitor the apoptosis process and to indicate the end point of PDT. Tang *et al.* reported another work on apoptosis monitoring using the natural AIE theranostic probe berberine (Fig. 8B).[68] Upon continuous light irradiation; berberine displays a strong photosensitizing property by generating large amounts of ROS, which initiate cancer cell apoptosis. The study shows that berberine not only acts as a photosensitizer in cancer photodynamic therapy, but also acts as a bioimaging probe to reflect the apoptosis process. Throughout the light irradiation process, the staining site of berberine migrates from mitochondria to the nucleus, which indicates the occurrence of apoptosis. Both AIE photosensitizers act as a self-reporter to cell apoptosis initiation, which also depicts a new way of visualizing the photodynamic therapy process.

Aside from self-reporting AIE photosensitizers, Tang *et al.* developed an AIE bioimaging probe, namely TVQE, capable of labeling mitochondria with red fluorescence (Fig. 8C).[69] At the same time, hydrophilic TVQE can be hydrolyzed by intracellular esterase and form hydrophobic TVQ, which shows blue emission and shifts the labeling site from mitochondria to lipid droplets. As esterase activity reflects cell viability conditions, in which the labeling location and color shifts of this esterase dependent AIEgen structural changes can be used to monitor cell conditions, especially for cell apoptosis that often experiences declined esterase activity. As a result, blue emission is much weaker in apoptotic cells than in live cells. In the late apoptotic stage, no blue emission was found, while strong red emission was detected due to the inactivated esterase activity. This AIE imaging probe can then be used to visualize the different stages of apoptosis, from early to late apoptosis, by monitoring the blue and red emission intensity changes. Another reported strategy to monitor apoptosis is to evaluate caspase 3/7 by AIE bioprobes. Meade *et al.* reported a caspase responsive probe that can simultaneously exhibit a fluorescence-magnetic resonance turn on response to caspase 3/7.[70] The caspase probe contains DOTA-Gd (II) chelate for providing magnetic resonance signal, tetraphenylethylene as the AIEgen for fluorescence signal and DEVD peptide as a substrate for caspase-3/7. The water-soluble peptide DEVD is

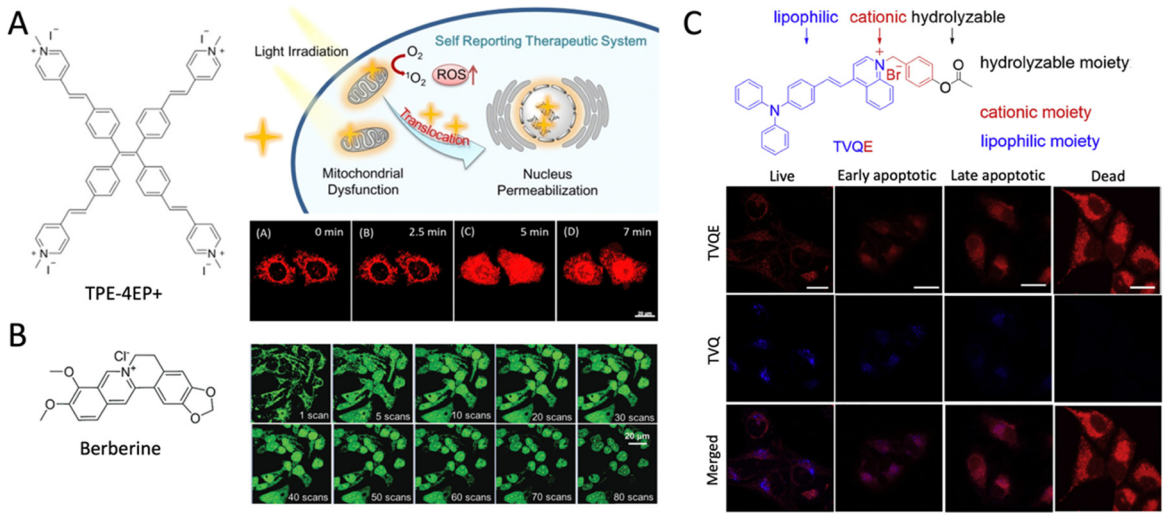

Fig. 8 AIE probes as fluorescent tracers of cell apoptosis. (A) TPE-4EP+ as an *in situ* monitoring apoptosis process by a self-reporting photosensitizer. Reprinted with permission from ref. 67. Copyright 2019 American Chemical Society. (B) Berberine as an AIE-active self-reporting cancer theranostic probe from natural herbs. Reprinted with permission from ref. 68. Copyright 2019 The Royal Society of Chemistry. (C) TVQE as single AIEgen to image dual organelles and evaluate cell apoptotic conditions. Reprinted with permission from ref. 69. Copyright 2020 Elsevier Ltd.

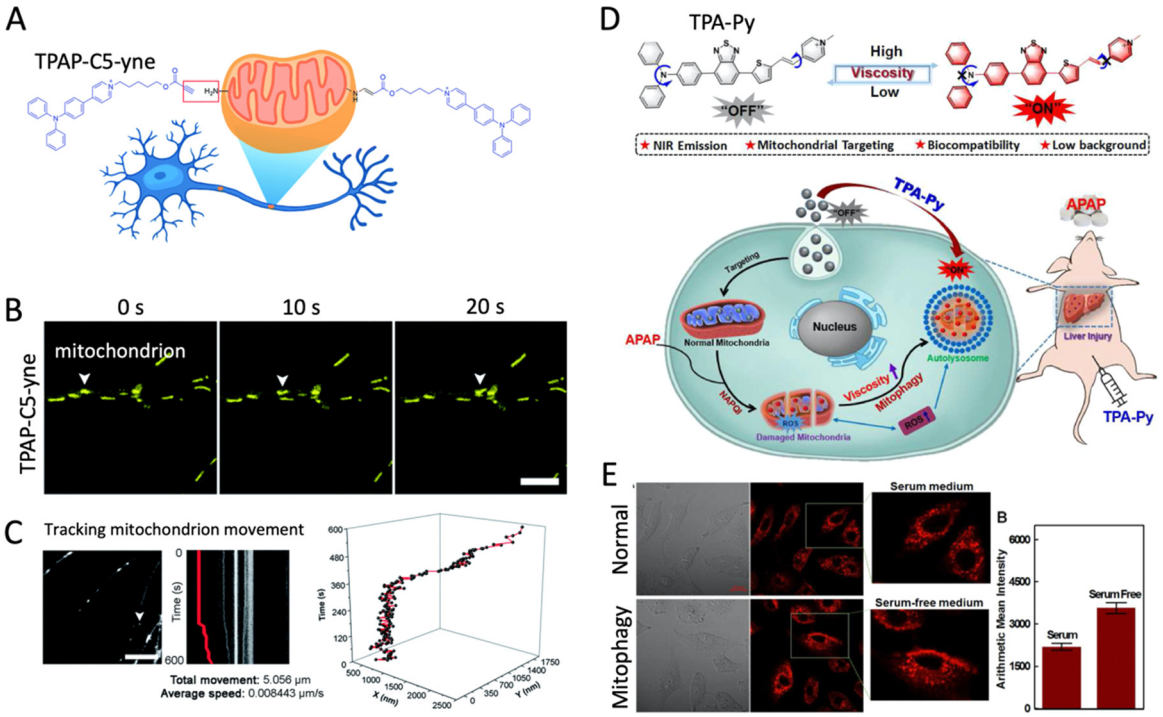

Fig. 9 AIE probes to trace mitochondrial movement and mitophagy. (A) TPAP-C5-yne as bioconjugatable and photostable AIEgen to precisely perform long-term tracking of mitochondria in neurons. (B) Confocal images of neuronal cells stained with TPAP-C5-yne. Scale bar: 5 mm. (C) Real-time image obtained using an EM-CCD camera, with a white arrow indicating a mitochondrion. Kymograph generated from the indicated mitochondrion. Scale bar: 10 mm. Three-dimensional diagram tracking the movement of a mitochondrion in a neuron. Reprinted with permission from ref. 71. Copyright 2022 The Royal Society of Chemistry. (D) TPA-Py as a near-infrared viscosity probe to image mitophagy during liver injury. (E) Fluorescence images of mitochondria viscosity in A549 cells incubated with 5 mM TPA-Py in a serum-containing culture medium and serum-free medium. Reprinted with permission from ref. 74. Copyright 2021 Elsevier Ltd.

cleaved upon responding to caspase 3/7, in which the remaining Gd(III)-AIEgen conjugate aggregates leads to an increase in fluorescence-magnetic signals, thereby successfully monitoring cell apoptosis.

Mitochondrial movement and mitophagy

Mitochondria, known as the powerhouse of cells, is an important organelle in eukaryotes. Having a double membrane structure, mitochondria are responsible for generating adenosine triphosphate used throughout the cell as a source of energy. In addition, mitochondria are associated with certain important bioprocesses, including mitophagy and mitochondrial injury-initiated apoptosis. Mitophagy plays a crucial role in maintaining intracellular homeostasis by removing dysfunctional mitochondria and recycling their constituents in a lysosome-degradative pathway. Therefore, studying and tracking mitochondria dynamics and mitochondrial-related bioprocess are attractive research directions. Tang *et al.* designed a mitochondrial tracking AIE bioprobe, namely TPAP-C5-yne, which can accurately analyze the motion of a single mitochondrion in live primary hippocampal neurons and the long-term tracking of mitochondria for up to 7 days in live neurons (Fig. 9A–C).[71] The mitochondrial labeling mechanism of TPAP-C5-yne is based on bioconjugation between the alkyne unit of AIEgen and the amine groups existing on mitochondria in neurons. With the covalent binding to mitochondria, TPAP-C5-yne can precisely perform long-term tracking of mitochondrial movement without dye leakages, which opens a new window in developing fluorescent probes to study the transport of mitochondria in live neurons.

Despite the mitochondrial movement, monitoring the mitochondrial membrane potential difference is of interest as a critical parameter representing mitochondrial function and cellular activities. Dong *et al.* presented a novel mitochondria-lysosome migration AIE probe, CSP, for *in situ* real-time tracking of mitochondrial membrane potential variations.[72] This cationic probe can image mitochondria with normal mitochondrial membrane potential with photostability and without washing procedures. When MMP decreases, CSP is then released from mitochondria and moves to label lysosomes. CSP can then return to mitochondria labeling with the recovery of mitochondrial membrane potential. Furthermore, the average colocalization coefficient obtained from the collaboration of CSP and commercial lysosome tracking dye can be used as an accurate parameter to monitor mitochondrial membrane potential dynamics in cells.

Aside from studying mitochondrial dynamics in cells, Dong *et al.* unveil the possibilities of AIEgens as tracking probes to the mitophagy process.[73] In this work, mitochondria-immobilized NIR-emissive AIE probe, CS-Py-BC, allows

for an off–on fluorescence response to viscosity that enables real-time monitoring of viscosity variation during mitophagy. Positively charged CS-Py-BC has mitochondria-specific targeting properties by the electrostatic interaction with the negatively charged mitochondrial membrane. Moreover, the benzyl chloride group participated in mitochondria immobilization through nucleophilic substitution with thiol groups in mitochondrial proteins. As one of the typical autophagy processes, mitophagy refers to dysfunctional mitochondria being encircled into autophagosomes, followed by being fused by lysosomes to form autolysosomes for further degradation, in which mitochondrial viscosity increases during the process. Based on this phenomenon, CS-Py-BC allows the real-time monitoring of viscosity changes during starvation or rapamycin-induced mitophagy. Besides, Li and Yu *et al.* reported another viscosity-dependent mitophagy monitoring AIE probe, TPA-Py (Fig. 9D and E).[74] Apart from having near-infrared emission, good water-solubility, and a mitochondrial targeting property, TPA-Py consist of two rotatable triphenylamine that enable the AIE property to be sensitive to viscosity changes. Due to the effective restriction of structural rotors, the probe displays string fluorescence upon meeting environmental viscosity increase. This photophysical property then allows TPA-Py to be used to study the viscosity changes in drug-induced liver injury with autophagy. Having the specific mitochondrial targeting property and high sensitivity to viscosity changes, both AIEgens can be promising imaging probes for mitophagy-related clinical research. Another mitochondrial-associated bioprocess is apoptosis. Li and Gao *et al.* reported an AIEgen TTVPHE, which is not only a mitochondria-anchoring photosensitizer but also an imaging probe to monitor the mitochondrial damaging process during apoptosis under photodynamic therapy.[75] In this work, the morphology of mitochondria under PDT was monitored *in situ* with excellent contrast and bright emission by TTVPHE aggregates. With prolonged light irradiation time, it is found that the morphology of mitochondria changed from rod to swelling circles, which indicates the injury of mitochondria.

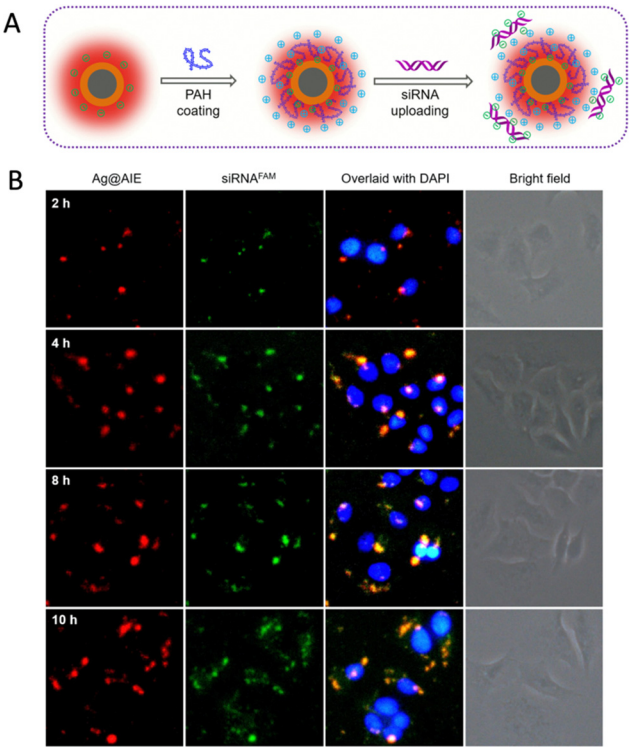

Fig. 10 Ag@AIE core shell nanocarriers for efficient and real-time monitoring of small interfering RNA delivery in cancer cells. (A) Schematic illustration of the layer-by-layer process for siRNA uploading. First, the cationic PAH polymer is wrapped outside the core@shell nanoparticle. The anionic siRNA is then uploaded *via* electrostatic interaction. (B) Confocal images showing the real-time tracing of siRNA delivery in cancer cells at 2 h, 4 h, 8 h, and 10 h post-incubation. Images were captured under a 63× oil objective. Reprinted with permission from ref. 76. Copyright 2019 American Chemical Society.

Drug and gene delivery

Real-time tracking of a drug and gene delivery system in cells is important to study the pharmaceutical mechanism and reveal the effectiveness of a therapy. One particularly popular research method is employing small interfering RNA for sequence-specific suppression of genes in disease therapeutics. Tang and Li *et al.* designed and fabricated Ag@AIE core@shell nanocarriers that carry small interfering RNA in the cancer cell, which can achieve target gene knockdown and cancer cell inhibition (Fig. 10).[76] In this work, the gene delivery process through AIE carrier to cells was successfully monitored by observing the fluorescence signal dynamics of both small interfering RNA and AIE nanocarriers. Through long-term fluorescence tracking, a good overlapping signal between small interfering RNA and AIE nanocarrier was found throughout the plasma membrane entry process, which indicates the very good protection of small interfering RNA from enzyme degradation by endocytosis. After a longer incubation time, the observed gradual decrease in colocalization efficiency of two emission signals indicates the separation of small interfering RNA from Ag@AIE nanocarrier, which indicates the gradual release of small interfering RNA for subsequent RNA interference in cancer cells.

Regarding gene delivery to cells, another work reported by Dai and Wang *et al.* also reported the use of AIE property in nanocarriers to monitor the small interfering RNA delivery process in cells.[77] The AIE moiety Py-TPE in the studied prodrug nanoparticle Py-TPE/siRNA@PMP facilitates drug entry in ovarian cancer cells, which indicates successful delivery of small interfering RNA into the cell for further cancer therapy. The inherent AIE properties contribute to the achievement of real-time intracellular tracking of gene delivery and long-term tumor tissue imaging, showing exceptional improvements in biocompatibility and delivery efficiency compared to commercial transfection reagents. Ji and Jin *et al.* reported a theranostic gemcitabine prodrug with self-monitoring therapeutic effectiveness properties.[78] The reported prodrug consists of an AIE moiety that can only light-up once the GFLG peptide in the drug is hydrolyzed by overexpressed cathepsin B in

cancer cells, followed by the release of the active drug gemcitabine and the apoptotic probe TPE-DEVD-RGD, in which DEVD peptide is then cleaved by the apoptosis activated by gemcitabine. Therefore, strong blue fluorescence can be observed from the TPE residues with aggregate formation, which indicates the successful initiation of cancer cell apoptotic therapy. Another work published by Gao and Han *et al.* fabricated doxorubicin-loaded polyethylene glycol-*block*-peptide (FFKY)-*block*-tetraphenylethylene (PEG-Pep-TPE/DOX) nanoparticles for cancer therapy and real-time drug release monitoring.[79] The nanoparticle contains AIEgen TPE-CHO that becomes a fluorescence resonance energy transfer pair with the entrapped antitumor drug DOX to detect the release of drugs dynamically. Overall, the above works provide new horizons for evaluating disease therapy efficiency through the real-time tracking of drug delivery and drug release in cells by incorporating AIE probes.

Nucleus division monitoring

The cell nucleus, which contains nearly all cell DNA wrapped by two layers of the nuclear membrane, is an important and largest organelle in animal cells. With the DNA and enzymes found to cause malignant proliferation, the nucleus is always considered an ideal target for cancer theranostics. However, the complex structure and intact barrier of the cell nucleus put great challenges to designing bioimaging and therapeutic agents targeting the nucleus. Recently, Liu and Mao *et al.* designed and synthesized an AIE self-reporting photosensitizer, MeTPAE, that targets cell nuclei (Fig. 11).[80] MeTPAE can bind to nucleic acids with bright fluorescence, facilitating the long-term monitoring of cell nucleus division process. In addition, MeTPAE has different functional groups to inhibit histone deacetylase and telomerase activity in the nucleus. The AIE fluorescent property of MeTPAE helps visualize the nucleus division status after a certain incubation time. The confocal imaging showed that most cells were undergoing multinucleated stater or G2 phase of mitosis, which reflected that the cells treated by MeTPAE were hindered from dividing. This work demonstrated the feasibility of AIEgens as dual agents to monitor cell nuclear division, as well as to visualize the effectiveness of the corresponding nuclear enzyme inhibitors as part of a cancer cell ablation process.

Intracellular bacteria monitoring

Bacterial infections and the rise of antibiotic resistance are threatening human health. This problem is even worse for intracellular bacteria, which are particularly difficult to eliminate with antibiotics. These bacteria are only visualized with multiple cellular treatments, which require profound and effective diagnosis and treatment to tackle the problem. To solve this problem, Liu *et al.* reported an AIE probe named TPEPy-D-Ala that can target intracellular Gram-positive bacteria through a specific metabolic labeling process.[81] TPEPy-D-Ala consists of D-alanine and an AIE photosensitizer for fluorescence turn-on imaging of intracellular bacteria in host cells. The D-alanine in TPEPy-D-Ala participates in peptidoglycan metabolism in intracellular bacteria and becomes part of peptidoglycan building blocks. After that, the intramolecular motions of TPEPy-D-Ala are restricted, which results in enhanced fluorescence and allows the tracking of intracellular bacteria in living macrophages. Besides, Liu and Kong *et al.* reported another AIE theranostic probe TPACN-D-Ala that can also target intracellular Gram-positive bacteria with a similar labeling strategy to TPE-D-Ala.[82] With the help of the

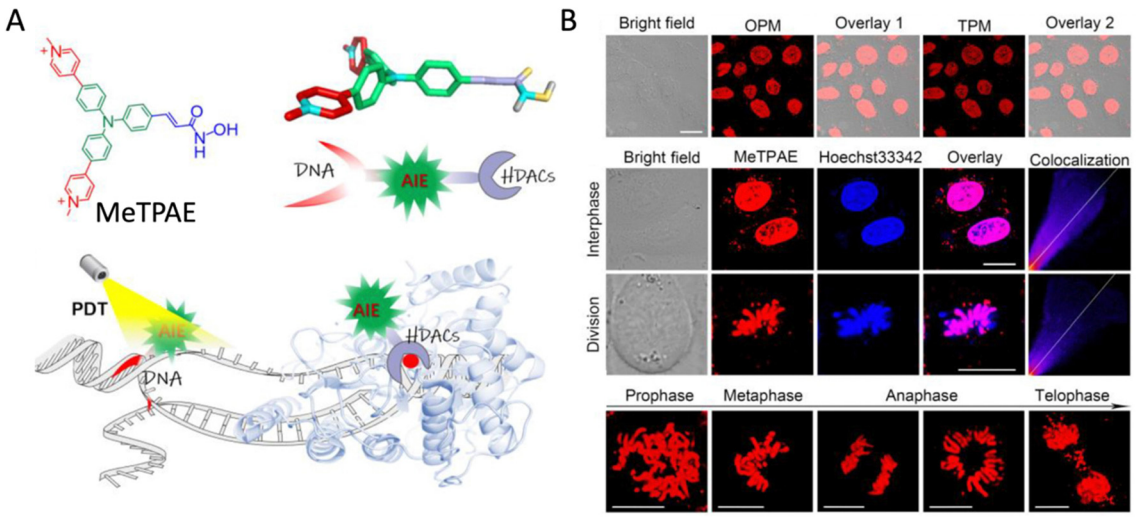

Fig. 11 AIE probes to specifically label cell nucleus and monitor nucleus division. MeTPAE as a nuclear-targeted AIE imaging probe to dynamically monitor chromosomes behavior during the cell cycle process. (A) Chemical structure of MeTPAE and schematic illustration of dual-responsive MeTPAE to nucleic acids and histone deacetylase, plus damaging telomere and nucleic acids by photodynamic therapy. (B) One-photon imaging (OPM) and two-photon imaging (TPM) of MeTPAE in HeLa cells. Scale bar: 20 μm. Confocal imaging and colocalization between MeTPAE and Hoechst 33342 in HeLa cells during cell interphase and division. Scale: 20 μm. Long-term tracing of chromosome dynamics by MeTPAE during the cell cycle process. Scale:10 μm. Reprinted with permission from ref. 80. Copyright 2022 Wiley-VCH.

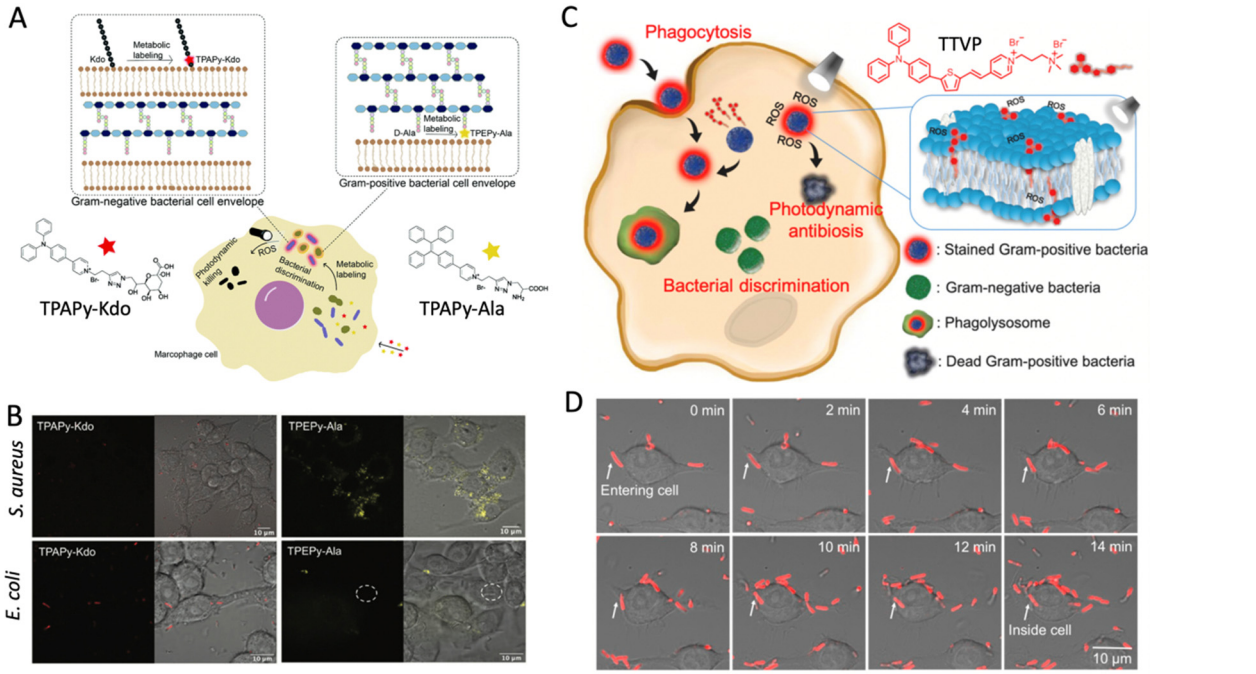

Fig. 12 Intracellular bacterial detection and phagocytosis monitoring using AIE probes. (A) TPEPy-Ala and TPAPy-Kdo as a metabolic bacteria-labeling bioprobe to visualize various species of intracellular bacteria. (B) Confocal images of intracellular *S. aureus* incubated with TPEPy-Ala and TPAPy-Kdo for 1 h. Confocal images of intracellular *E. coli* incubated with TPEPy-Ala and TPAPy-Kdo for 2 h. Reprinted with permission from ref. 83. Copyright 2022 The Royal Society of Chemistry. (C) TTVP as a bioimaging probe to monitor Gram-positive bacteria engulfed by macrophages during phagocytosis. (D) Long-term tracking confocal images showing TTVP-treated *B. subtilis* being entrapped by Raw 264.7 during phagocytosis. Reprinted with permission from ref. 84. Copyright 2020 Elsevier Ltd.

fluorescence diagnosis of intracellular environments, this work demonstrated a non-antibiotic strategy for further *in vivo* bacterial ablation. Besides intracellular bacterial tracing, monitoring the special types of intracellular bacteria is also important. Tang *et al.* reported two light-up metabolic AIE probes, namely TPEPy-Ala and TPAPy-Kdo, that can not only metabolically label and identify Gram-positive and Gram-negative bacteria with high signal-to-noise ratios but also visualize the bacteria internalized in cells. Gram-positive and Gram-negative bacteria experience two distinctly different cell envelope structures (Fig. 12A and B).[83] Gram-positive bacteria consist of a single thick layer of peptidoglycan on top of the bacterial membrane. In contrast, Gram-negative bacteria consist of a double-layered bacterial membrane with lipopolysaccharide on top of the outer membrane and a thin peptidoglycan layer in the middle of two membrane layers. Based on the bacteria structural difference, this work designs two AIE probes by incorporating D-alanine and 3-deoxy-D-manno-octulosonic acid (Kdo) respectively to TPEPy-Ala and TPAPy-Kdo. As a result, through metabolic labelling in bacteria, TPEPy-Ala successfully targets intracellular Gram-positive bacteria and TPAPy-Kdo could specifically discriminate intracellular Gram-negative bacteria. All the above work successfully demonstrated the feasibility of AIEgens as intracellular bacterial light-up probes. The high bacterial selectivity and AIE photophysical property could help trace and visualize intracellular bacteria.

Apart from the metabolic labeling approach, Tang *et al.* reported another AIEgen, TTVP, which can perform as an ideal intracellular Gram-positive bacterium targeting agent based on electrostatic attraction (Fig. 12C and D).[84] As bacteria express negatively charged envelope surfaces, adding a positively charged pyridinium moiety in the structural design of AIEgen can facilitate its electrostatic attraction to the bacterial surface, thus achieving simple and effective labeling. Furthermore, owing to the high photostability and signal-to-noise contrast of TTVP, this work demonstrated the successful tracing of TTVP-treated Gram-positive bacteria being engulfed by nearby phagocytosis. Liu *et al.* developed another AIE probe named TPEPy-Et, which also demonstrated excellent interaction with intracellular Gram-positive bacteria, due to electrostatic interaction between cationic TPEPy-Et and the anionic bacterial membrane.[85] The above works depict the applications of AIE bioprobes to trace and detect macrophage-engulfed bacteria, which also help to carry out further photodynamic antipathogenic therapy precisely.

Cellular response to bacteria entry

Phagocytosis, the very first immune response process triggered in a bacterial invasion, generally involves four steps: recognition of targets, activation of phagocytic signaling pathways, engulfment of targets, and phagosome maturation. As part of the cellular responses upon bacterial entry, real-time imaging

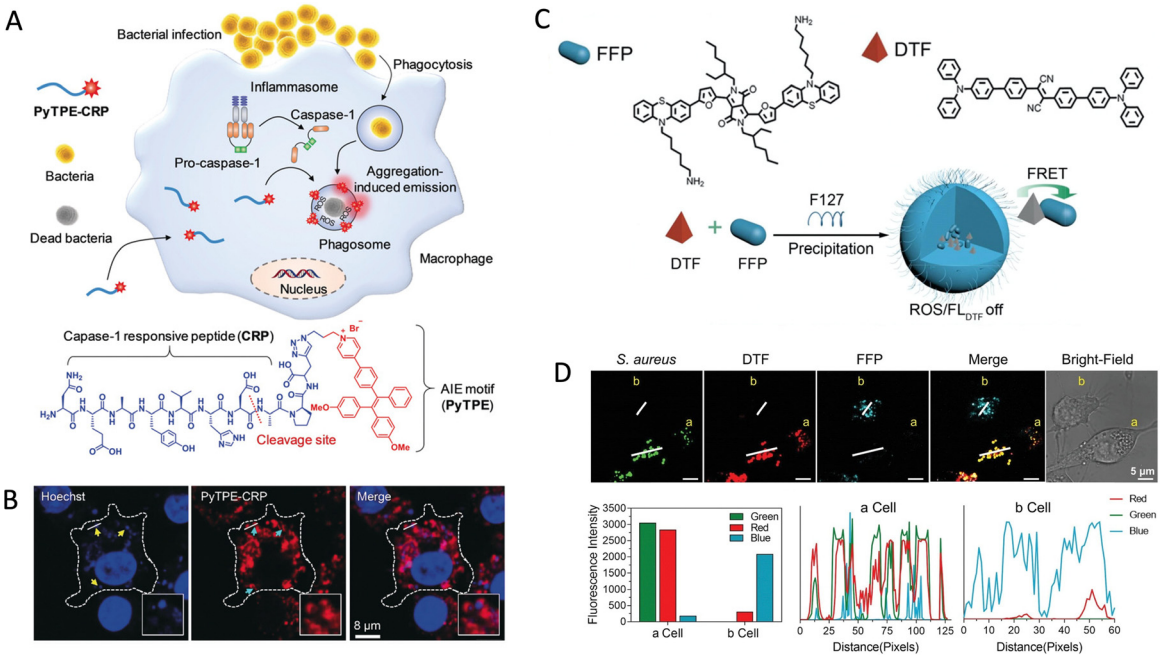

Fig. 13 AIE probes to monitor various cellular responses upon bacterial infection. (A) PyTPE-CRP as a macrophage-mediated intracellular bacterial infection diagnosis probe. Upon cleavage of the responsive moiety by caspase-1 during bacterial infection, PyTPE residues aggregate and give fluorescence in macrophages. (B) Confocal images of Raw 264.7 cells infected by *S. aureus* after incubation of PyTPE-CRP (red) for 60 min and Hoechst dye (blue), with yellow arrows indicating *S. aureus*, cyan arrows indicating phagosomes containing *S. aureus*. Reprinted with permission from ref. 87. Copyright 2019 Wiley-VCH. (C) DTF–FFP NPs as a dual color tracing probe to invade phagocytes. FFP dominates the fluorescence signal without bacterial invasion based on fluorescence resonance energy transfer. DTF dominates the fluorescence signal upon activation by HClO produced in a bacterial invaded phagocyte. (D) Confocal images of Raw 264.7 cells treated with DTF–FFP NPs and subsequent treatment of the cells with *S. aureus* for 1 h. *S. aureus* locations were indicated by the green fluorescence from SYTO 9. Fluorescence intensity analysis and line-scan profiles of a bacteria-infected cell (a cell) and non-infected cell (b cell). Reprinted with permission from ref. 88. Copyright 2020 Wiley-VCH.

of phagocytosis provides great help to unveil the phagocytic process and precisely develop diagnosis and treatment for phagocytosis-related diseases. Chen *et al.* reported a near-infrared plasma membrane-specific AIE probe, namely TBTCP, which can monitor phagocytosis by observing the labeled plasma membrane dynamics.[86] TBTCP, with excellent photostability and a high signal-to-noise ratio can achieve ultrafast and wash-free staining to the cell membrane of macrophages. In addition, TBTCP can be applied to real-time visualize topographic changes of macrophage membranes under osmolarity variations, as well as the early stages of phagocytosis of different species of bacteria. Aside from the early stage of phagocytosis, Liu *et al.* reported an AIE bioprobe, namely PyTPE-CRP, that can visualize bacterial-entrapping phagosomes (Fig. 13A and B).[87] Based on this property, macrophages can recognize the bacterial infection and activate caspase-1 to recruit bacteria into phagosomes. This AIEgen work is based on the composing enzyme-cleavable peptide (NEAYVHDAP) that acts as the responsive moiety to the presence of caspase-1 activation, thereby being cleaved between the amino acids Asp and Ala under pathogen invasion. After that, the left behind PyTPE-CRP residues could light up spontaneously in bacteria-containing phagosomes, owing to their insolubility in the aqueous environment and aggregate formation. Therefore, PyTPE-CRP acts as a fluorescent indicator to monitor the phagosome formation of macrophages under bacterial infection. On the other hand, Liu and Tang *et al.* developed an AIE nanoprobe that can image bacteria in phagocytes in the infected area (Fig. 13C and D).[88] In this work, DTF–FFP nanoparticles, as hypochlorous acid activable theranostic nanoprobes, are introduced to visualize and ablate bacteria in phagocytes. DTF–FFP nanoparticles are composed of FFP and DTF encapsulated by Pluronic F127. When the nanoprobe is delivered to normal cells, FFP quenches the fluorescence of DTF due to the fluorescence resonance energy transfer, which shows near-infrared emission by FFP. However, when the nanoprobe is delivered to the infection sites, FFP undergoes degradation owing to the stimulated release of hypochlorous acid in phagocytes, thereby, DTF emits red fluorescence. Therefore, this kind of AIE nanoprobe design strategy could visually classify bacteria-infected cells from normal cells by observing the emission color range under confocal microscopy. The above works demonstrate the possibility of visualizing and diagnosing the important cell response upon bacterial infection, which helps AIEgens to facilitate further carrying out highly sensitive and effective self-reported treatment to eliminate the cell-entrapped live pathogens, such as using photodynamic therapy.

4. Summary and prospects

Over the past, many AIE probes were successfully developed to visualize intracellular processes and monitor microenvironment

changes, which allow for a better understanding of physiological homeostasis. The working mechanism of RIM has made AIE probes excellent for intracellular studies because of the environmentally sensitive response. Other spectroscopic changes, such as TICT emission, ratiometric fluorescence, and fluorescence quenching, were also employed to transform intracellular information into visual images. The excellent photostability of AIE probes is another crucial feature that made it possible to monitor intracellular events and microenvironment changes dynamically. Although much progress has been made in real-time monitoring of the intracellular environment, there remains much room for improvement and future development. For instance, most reported AIE probes are limited to a specific organelle for monitoring intracellular environment changes. Moreover, more microenvironment parameters should also be investigated. Further development for *in vivo* monitoring of intracellular events is also desirable. In conclusion, AIE probes showed excellent advantages in overcoming the limitations of monitoring intracellular dynamics through their spectroscopic response to the environment, high photostability and biocompatibility, and resistance to photobleaching.

Conflicts of interest

There are no conflicts to declare.

Acknowledgements

The work described in this paper was supported by a fellowship award from the Research Grants Council of the Hong Kong Special Administrative Region, China (HKUST PDFS2122-6S01), the National Natural Science Foundation of China (52122317 and 22175120), the Research Grant Council of Hong Kong (16306620, 16303221, N_HKUST609/19 and C6014-20W), the Innovation and Technology Commission (ITC-CNERC14SC01), and the National Key Research, Development Program of China (2018YFE0190200).

References

1 R. Vadivambal and D. S. Jayas, *Bio-Imaging Principles, Techniques, and Applications*, CRC Press, 2016.
2 O. S. Wolfbeis, An overview of nanoparticles commonly used in fluorescent bioimaging, *Chem. Soc. Rev.*, 2015, **44**, 4743–4768.
3 H.-W. Liu, L. Chen, C. Xu, Z. Li, H. Zhang, X.-B. Zhang and W. Tan, Recent progresses in small-molecule enzymatic fluorescent probes for cancer imaging, *Chem. Soc. Rev.*, 2018, **47**, 7140–7180.
4 P. Zrazhevskiy, M. Sena and X. Gao, Designing multifunctional quantum dots for bioimaging, detection, and drug delivery, *Chem. Soc. Rev.*, 2010, **39**, 4326–4354.
5 N. Erathodiyil and J. Y. Ying, Functionalization of inorganic nanoparticles for bioimaging applications, *Acc. Chem. Res.*, 2011, **44**, 925–935.
6 L. Zhang and E. Wang, Metal nanoclusters: new fluorescent probes for sensors and bioimaging, *Nano Today*, 2014, **9**, 132–157.
7 C. Xu, J. Huang, Y. Jiang, S. He, C. Zhang and K. Pu, Nanoparticles with ultrasound-induced afterglow luminescence for tumour-specific theranostics, *Nat. Biomed. Eng.*, 2023, **7**, 298–312.
8 J. Huang, X. Chen, Y. Jiang, C. Zhang, S. He, H. Wang and K. Pu, Renal clearable polyfluorophore nanosensors for early diagnosis of cancer and allograft rejection, *Nat. Mater.*, 2022, **21**, 598–607.
9 P. Cheng and K. Pu, Molecular imaging and disease theranostics with renal-clearable optical agents, *Nat. Rev. Mater.*, 2021, **6**, 1095–1113.
10 Q. Miao, C. Xie, X. Zhen, Y. Lyu, H. Duan, X. Liu, J. V. Jokerst and K. Pu, Molecular afterglow imaging with bright, biodegradable polymer nanoparticles, *Nat. Biotechnol.*, 2017, **35**, 1102–1110.
11 A. Gandioso, R. Bresolí-Obach, A. Nin-Hill, M. Bosch, M. Palau, A. Galindo, S. Contreras, A. Rovira, C. Rovira, S. Nonell and V. Marchán, Redesigning the coumarin scaffold into small bright fluorophores with far-red to near-infrared emission and large stokes shifts useful for cell imaging, *J. Org. Chem.*, 2018, **83**, 1185–1195.
12 Y. Hong, J. W. Y. Lam and B. Z. Tang, Aggregation-induced emission, *Chem. Soc. Rev.*, 2011, **40**, 5361–5388.
13 J. Luo, Z. Xie, Z. Xie, J. W. Y. Lam, L. Cheng, H. Chen, C. Qiu, H. S. Kwok, X. Zhan, Y. Liu, D. Zhu and B. Z. Tang, Aggregation-induced emission of 1-methyl-1,2,3,4,5-pentaphenylsilole, *Chem. Commun.*, 2001, 1740–1741.
14 S. Song, Y. Wang, Y. Zhao, W. Huang, F. Zhang, S. Zhu, Q. Wu, S. Fu, B. Z. Tang and D. Wang, Molecular engineering of AIE luminogens for NIR-II/IIb bioimaging and surgical navigation of lymph nodes, *Matter*, 2022, **5**, 2847–2863.
15 Y. Qin, X. Chen, Y. Gui, H. Wang, B. Z. Tang and D. Wang, A self-assembled metallacage with second near-infrared aggregation-induced emission for enhanced multimodal theranostics, *J. Am. Chem. Soc.*, 2022, **144**, 12825–12833.
16 D. Yan, T. Li, Y. Yang, N. Niu, D. Wang, J. Ge, L. Wang, R. Zhang, D. Wang and B. Z. Tang, A water-soluble AIEgen for noninvasive diagnosis of kidney fibrosis *via* SWIR fluorescence and photoacoustic imaging, *Adv. Mater.*, 2022, **34**, 2206643.
17 D. Yan, M. Wang, Q. Wu, N. Niu, M. Li, R. Song, J. Rao, M. Kang, Z. Zhang, F. Zhou, D. Wang and B. Z. Tang, Multimodal imaging-guided photothermal immunotherapy based on a versatile NIR-II aggregation-induced emission luminogen, *Angew. Chem., Int. Ed.*, 2022, **61**, e202202614.
18 I. H. Madshus, Regulation of intracellular pH in eukaryotic cells, *Biochem. J.*, 1988, **250**, 1–8.
19 J. R. Casey, S. Grinstein and J. Orlowski, Sensors and regulators of intracellular pH, *Nat. Rev. Mol. Cell Biol.*, 2010, **11**, 50–61.
20 J. Zhuang, Y. Yu, R. Su, Q. Ma, N. Li and N. Zhao, A ratiometric AIE probe for dual color imaging lipid droplets and lysosomes and real-time quantitative monitoring lipophagy, *Dyes Pigm.*, 2022, **208**, 110809.

21 S. Chen, Y. Hong, Y. Liu, J. Liu, C. W. T. Leung, M. Li, R. T. K. Kwok, E. Zhao, J. W. Y. Lam, Y. Yu and B. Z. Tang, Full-Range Intracellular pH sensing by an aggregation-induced emission-active two-channel ratiometric fluorogen, *J. Am. Chem.*, 2013, **135**, 4926–4929.
22 Y. Gu, Z. Zhao, G. Niu, H. Zhang, Y. Wang, R. T. K. Kwok, J. W. Y. Lam and B. Z. Tang, Visualizing semipermeability of the cell membrane using a pH-responsive ratiometric AIEgen, *Chem. Sci.*, 2020, **11**, 5753–5758.
23 N. Zhao, Y. Li, W. Yang, J. Zhuang, Y. Li and N. Li, Multifunctional pyrazoline based AIEgens: real-time tracking and specific protein ''fishing'' of lipid droplets, *Chem. Sci.*, 2019, **10**, 9009–9016.
24 S. Zhang, T. Wang, X. Wang, W. Liao, X. Wang, Y. Yuan, G. Chen and X. Jia, A novel aggregation-induced emission fluorescent probe with large Stokes shift for sensitive detection of pH changes in live cells, *Luminescence*, 2022, **37**, 2139–2144.
25 Q. Li, Z. Niu, X. Nan and E. Wang, An AIE-Active probe for detection and bioimaging of pH values based on lactone hydrolysis reaction, *J. Fluoresc.*, 2022, **32**, 1611–1617.
26 J. L. Roti Roti, Cellular responses to hyperthermia (40–46 °C): cell killing and molecular events, *Int. J. Hyperth.*, 2008, **24**, 3–15.
27 J. R. Lepock, How do cells respond to their thermal environment?, *Int. J. Hyperth.*, 2005, **21**, 681–687.
28 B. Saha, B. Ruidas, S. Mete, C. D. Mukhopadhyay, K. Bauri and P. De, AIE-active non-conjugated poly(N-vinylcaprolactam) as a fluorescent thermometer for intracellular temperature imaging, *Chem. Sci.*, 2020, **11**, 141–147.
29 S. Lin, H. Pan, L. Li, R. Liao, S. Yu, Q. Zhao, H. Sun and W. Huang, AIPE-active platinum(ii) complexes with tunable photophysical properties and their application in constructing thermosensitive probes used for intracellular temperature imaging, *J. Mater. Chem. C*, 2019, **7**, 7893–7899.
30 K.-F. Chen, S. Liu, M. Gao, J. Wang, Y. Wang, X. Chen, Y. Chen, L. Ren, H. Zhang, Y.-G. Jia and X. X. Zhu, AIE-active and thermoresponsive alternating polyurethanes of bile acid and PEG for cell imaging, *ACS Appl. Polym. Mater.*, 2019, **1**, 2973–2980.
31 L. Meng, S. Jiang, M. Song, F. Yan, W. Zhang, B. Xu and W. Tian, TICT-based near-infrared ratiometric organic fluorescent thermometer for intracellular temperature sensing, *ACS Appl. Mater. Interfaces*, 2020, **12**, 26842–26851.
32 J. L. Lee and C. H. Streuli, Integrins and epithelial cell polarity, *J. Cell Sci.*, 2014, **127**, 3217–3225.
33 J. P. Campanale, T. Y. Sun and D. J. Montell, Development and dynamics of cell polarity at a glance, *J. Cell Sci.*, 2017, **130**, 1201–1207.
34 C. Wang, J. Wang, K. Xue, M. Xiao, K. Wu, S. Lv, B. Hao and C. Zhu, Polarity-sensitive fluorescent probe for reflecting the packing degree of bacterial membrane lipids, *Anal. Chem.*, 2022, **94**, 3303–3312.
35 C. Zhou, M. Jiang, J. Du, H. Bai, G. Shan, R. T. K. Kwok, J. H. C. Chau, J. Zhang, J. W. Y. Lam, P. Huang and B. Z. Tang, One stone, three birds: one AIEgen with three colors for fast differentiation of three pathogens, *Chem. Sci.*, 2020, **11**, 4730–4740.
36 T. Yang, Y. Zuo, Y. Zhang, Z. Gou, X. Wang and W. Lin, AIE-active polysiloxane-based fluorescent probe for identifying cancer cells by locating lipid drops, *Anal. Chim. Acta*, 2019, **1091**, 88–94.
37 C. Lai, Y. Zhao, Y. Liang, X. Zou and W. Lin, BF_2 group chelated AIE fluorescent probe for polarity mapping of lipid droplets in cells and in vivo, *Spectrochim. Acta A Mol. Biomol. Spectrosc.*, 2022, **268**, 120637.
38 M. Li, W. Fang, B. Wang, Y. Du, Y. Hou, L. Chen, S. Cui, Y. Li and X. Yan, A novel dual-site ICT/AIE fluorescent probe for detecting hypochlorite and polarity in living cells, *New J. Chem.*, 2021, **45**, 21406–21414.
39 T. C. Owyong, P. Subedi, J. Deng, E. Hinde, J. J. Paxman, J. M. White, W. Chen, B. Heras, W. W. H. Wong and Y. Hong, A molecular chameleon for mapping subcellular polarity in an unfolded proteome environment, *Angew. Chem., Int. Ed.*, 2020, **59**, 10129–10135.
40 E. O. Puchkov, Intracellular viscosity: methods of measurement and role in metabolism, *Biochem. Moscow Suppl. Ser. A*, 2013, **7**, 270–279.
41 W. J. Shi, J. Yang, Y. F. Wei, X. T. Li, X. H. Yan, Y. Wang, H. Leng, L. Zheng and J. W. Yan, Novel cationic meso-CF_3 BODIPY-based AIE fluorescent rotors for imaging viscosity in mitochondria, *Chem. Commun.*, 2022, **58**, 1930–1933.
42 Y. Wang, Y. Qiu, A. Sun, Y. Xiong, H. Tan, Y. Shi, P. Yu, G. Roy, L. Zhang and J. Yan, Dual-functional AIE fluorescent probes for imaging β-amyloid plaques and lipid droplets, *Anal. Chim. Acta*, 2020, **1133**, 109–118.
43 Y. Zheng, Y. Ding, X. Zheng, C. Zhang, Y. Zhang, Y. Xiang and A. Tong, Long-term dynamic imaging of cellular processes using an AIE lipid order probe in the dual-color mode, *Anal. Chem.*, 2021, **93**, 10272–10281.
44 Y. Dou, Kenry, J. Liu, F. Zhang, C. Cai and Q. Zhu, 2-Styrylquinoline-based two-photon AIEgens for dual monitoring of pH and viscosity in living cells, *J. Mater. Chem. B*, 2019, **7**, 7771–7775.
45 Y. Zhang, S. Wang, X. Wang, Q. Zan, X. Yu, L. Fan and C. Dong, Monitoring of the decreased mitochondrial viscosity during heat stroke with a mitochondrial AIE probe, *Anal. Bioanal. Chem.*, 2021, **413**, 3823–3831.
46 C. F. Mueller, K. Laude, J. S. McNally and D. G. Harrison, ATVB in focus: redox mechanisms in blood vessels, *Arterioscler., Thromb., Vasc. Biol.*, 2005, **25**, 274–278.
47 J. H. C. Chau, R. Zhang, M. M. S. Lee, K. W. K. Lam, E. Y. Yu, J. W. Y. Lam, R. T. K. Kwok and B. Z. Tang, A ratiometric theranostic system for visualization of ONOO− species and reduction of drug-induced hepatotoxicity, *Biomater. Sci.*, 2022, **10**, 1083–1089.
48 B. Guo, W. Shu, W. Liu, H. Wang, S. Xing, J. Chen and X. Zhang, Mitochondria-specific ultrasensitive ratiometric AIE probe for imaging endogenous peroxynitrite, *Sens. Actuators, B*, 2021, **344**, 130206.
49 M. Xue, H. Wang, J. Chen, J. Ren, S. Chen, H. Yang, R. Zeng, Y. Long and P. Zhang, Ratiometric fluorescent sensing of

endogenous hypochlorous acid in lysosomes using AIE-based polymeric nanoprobe, *Sens. Actuators, B*, 2019, **282**, 1–8.

50 J. Shen, K. Shao, W. Zhang and Y. He, Hypoxia-triggered in situ self-assembly of a charge switchable azo polymer with AIEgens for tumor imaging, *ACS Macro Lett.*, 2021, **10**, 702–707.

51 C. Xu, H. Zou, Z. Zhao, P. Zhang, R. T. K. Kwok, J. W. Y. Lam, H. H. Y. Sung, I. D. Williams and B. Z. Tang, A new strategy toward ''simple'' water-soluble AIE probes for hypoxia detection, *Adv. Funct. Mater.*, 2019, **29**, 1903278.

52 J. Li, W. Liu, Z. Li, Y. Hu, J. Yang and J. Li, PEGylated AIEgen molecular probe for hypoxia-mediated tumor imaging and photodynamic therapy, *Chem. Commun.*, 2021, **57**, 4710–4713.

53 Y. Tang, X. Wang, G. Zhu, Z. Liu, X.-M. Chen, H. K. Bisoyi, X. Chen, X. Chen, Y. Xu, J. Li and Q. Li, Hypoxia-responsive photosensitizer targeting dual organelles for photodynamic therapy of tumors, *Small*, 2022, 2205440.

54 M. Li, H. Li, Q. Wu, N. Niu, J. Huang, L. Zhang, Y. Li, D. Wang and B. Z. Tang, Hypoxia-activated probe for NIR fluorescence and photoacoustic dual-mode tumor imaging, *iScience*, 2021, **24**, 102261.

55 H. J. Forman, H. Zhang and A. Rinna, Glutathione: Overview of its protective roles, measurement, and biosynthesis, *Mol. Aspects Med.*, 2009, **30**, 1–12.

56 Y. Gu, Z. Zhao, G. Niu, R. Zhang, H. Zhang, G.-G. Shan, H.-T. Feng, R. T. K. Kwok, J. W. Y. Lam, X. Yu and B. Z. Tang, Ratiometric detection of mitochondrial thiol with a two-photon active AIEgen, *ACS Appl. Bio Mater.*, 2019, **2**, 3120–3127.

57 W. Wang, M. Ji, J. Chen and P. Wang, A novel turn-on type AIE fluorescent probe for highly selective detection of cysteine/homocysteine and its application in living cells, *Talanta*, 2022, **239**, 123091.

58 Y. H. Zhang, X. Li, L. Huang, H. S. Kim, J. An, M. Lan, Q.-Y. Cao and J. S. Kim, AIE based GSH activatable photosensitizer for imaging-guided photodynamic therapy, *Chem. Commun.*, 2020, **56**, 10317–10320.

59 A. N. Ramya, M. M. Joseph, V. Karunakaran, C. V. S. Ahammed, A. Samanta and K. K. Maiti, An efficient molecular luminophore based on tetraphenylethylene (TPE) enabling intracellular detection and therapeutic benefits of hydrogen sulfide in Alzheimer's disease, *Sens. Actuators, B*, 2022, **355**, 131118.

60 Y. Yuan, S. Xu, C.-J. Zhang, R. Zhang and B. Liu, Dual-targeted activatable photosensitizers with aggregation-induced emission (AIE) characteristics for image-guided photodynamic cancer cell ablation, *J. Mater. Chem. B*, 2016, **4**, 169–176.

61 L. Dong, M.-Y. Zhang, H.-H. Han, Y. Zang, G.-R. Chen, J. Li, X.-P. He and S. Vidal, A general strategy to the intracellular sensing of glycosidases using AIE-based glycoclusters, *Chem. Sci.*, 2022, **13**, 247–256.

62 K. Gu, W. Qiu, Z. Guo, C. Yan, S. Zhu, D. Yao, P. Shi, H. Tian and W.-H. Zhu, An enzyme-activatable probe liberating AIEgens: on-site sensing and long-term tracking of β-galactosidase in ovarian cancer cells, *Chem. Sci.*, 2019, **10**, 398–405.

63 Z. Zhu, Q. Wang, X. Chen, Q. Wang, C. Yan, X. Zhao, W. Zhao and W.-H. Zhu, An enzyme-activatable aggregation-induced-emission probe: intraoperative pathological fluorescent diagnosis of pancreatic cancer *via* specific cathepsin E, *Adv. Mater.*, 2022, **34**, 2107444.

64 Y. Wu, Y. Gao, J. Su, Z. Chen and S. Liu, In situ detection of intracellular tissue transglutaminase based on aggregation-induced emission, *Chem. Commun.*, 2020, **56**, 9008–9011.

65 C. Xiang, M. Dirak, Y. Luo, Y. Peng, L. Cai, P. Gong, P. Zhang and S. Kolemen, A responsive AIE-active fluorescent probe for visualization of acetylcholinesterase activity in vitro and in vivo, *Mater. Chem. Front.*, 2022, **6**, 1515–1521.

66 Y. Xu, M. Cui, W. Zhang, T. Liu, X. Ren, Y. Gu, C. Ran, J. Yang and P. Wang, A sulfatase-activatable AIEgen nanoprobe for inhalation imaging-guided surgical excision of lung cancer, *Chem. Eng. J.*, 2022, **428**, 132514.

67 T. Zhang, Y. Li, Z. Zheng, R. Ye, Y. Zhang, R. T. K. Kwok, J. W. Y. Lam and B. T. Tang, In situ monitoring apoptosis process by a self-reporting photosensitizer, *J. Am. Chem. Soc.*, 2019, **141**, 5612–5616.

68 M. M. S. Lee, L. Zheng, B. Yu, W. Xu, R. T. K. Kwok, J. W. Y. Lam, F. Xu, D. Wang and B. Z. Tang, A highly efficient and AIE-active theranostic agent from natural herbs, *Mater. Chem. Front.*, 2019, **3**, 1454–1461.

69 R. Zhang, G. Niu, Z. Liu, J. H. C. Chau, H. Su, M. M. S. Lee, Y. Gu, R. T. K. Kwok, J. W. Y. Lam and B. Z. Tang, Single AIEgen for multiple tasks: imaging of dual organelles and evaluation of cell viability, *Biomaterials*, 2020, **242**, 119924.

70 H. Li, G. Parigi, C. Luchinat and T. J. Meade, Bimodal Fluorescence-Magnetic Resonance Contrast Agent for Apoptosis Imaging, *J. Am. Chem. Soc.*, 2019, **141**, 6224–6233.

71 H. Park, G. Niu, C. Wu, C. Park, H. Liu, H. Park, R. T. K. Kwok, J. Zhang, B. He and B. Z. Tang, Precise and long-term tracking of mitochondria in neurons using a bioconjugate and photostable AIE luminogen, *Chem. Sci.*, 2022, **13**, 2965–2970.

72 L. Fana, J. Ge, Q. Zan, X. Wang, S. Wang, Y. Zhang, W. Dong, S. Shuang and C. Dong, Real-time tracking the mitochondrial membrane potential by a mitochondria-lysosomes migration fluorescent probe with NIR-emissive AIE characteristics, *Sens. Actuators, B*, 2021, **327**, 128929.

73 X. Wang, L. Fan, S. Wang, Y. Zhang, F. Li, Q. Zan, W. Lu, S. Shuang and C. Dong, Real-time monitoring mitochondrial viscosity during mitophagy using a mitochondria-immobilized near-infrared aggregation-induced emission probe, *Anal. Chem.*, 2021, **93**, 3241–3249.

74 C. Peng, X. Ma, D. Lin, X. Feng, H. Yu and Y. Li, A novel near-infrared viscosity probe based on the synergistic effect of AIE property and molecular rotors for mitophagy imaging during liver injury, *Anal. Chim. Acta*, 2021, **1187**, 339146.

75 T. Zhou, J. Zhu, D. Shang, C. Chai, Y. Li, H. Sun, Y. Li, M. Gao and M. Li, Mitochondria-anchoring and AIE-active photosensitizer for self-monitored cholangiocarcinoma therapy, *Mater. Chem. Front.*, 2020, **4**, 3201–3208.

76 X. He, F. Yin, D. Wang, L. H. Xiong, R. T. K. Kwok, P. F. Gao, Z. Zhao, J. W. Y. Lam, K.-T. Yong, Z. Li and B. Z. Tang, AIE featured inorganic–organic core@ shell nanoparticles for high-efficiency siRNA delivery and real-time monitoring, *Nano Lett.*, 2019, **19**, 2272–2279.

77 J. Wu, Q. Wang, X. Dong, M. Xu, J. Yang, X. Yi, B. Chen, X. Dong, Y. Wang, X. Lou, F. Xia, S. Wang and J. Dai, Biocompatible AIEgen/p-glycoprotein siRNA@reduction-sensitive paclitaxel polymeric prodrug nanoparticles for overcoming chemotherapy resistance in ovarian cancer, *Theranostics*, 2021, **11**, 3710–3724.

78 H. Han, W. Teng, T. Chen, J. Zhao, Q. Jin, Z. Qin and J. Ji, A cascade enzymatic reaction activatable gemcitabine prodrug with an AIE-based intracellular light-up apoptotic probe for in situ self-therapeutic monitoring, *Chem. Commun.*, 2017, **53**, 9214–9217.

79 T. Wang, Q. Wei, Z. Zhang, M. Lin, J. Chen, Y. Zhou, N. Guo, X. Zhong, W. Xu, Z. Liu, M. Han and J. Gao, AIE/FRET-based versatile PEG-Pep-TPE/DOX nanoparticles for cancer therapy and real-time drug release monitoring, *Biomater. Sci.*, 2020, **8**, 118–124.

80 K. Wang, L. Liu, D. Mao, M. Hou, C. Tan, Z. Mao and B. Liu, A nuclear-targeted AIE photosensitizer for enzyme inhibition and photosensitization in cancer cell ablation, *Angew. Chem., Int. Ed.*, 2022, **61**, e202114600.

81 F. Hu, G. Qi, Kenry, D. Mao, S. Zhou, M. Wu, W. Wu and B. Liu, Visualization and in situ ablation of intracellular bacterial pathogens through metabolic labeling, *Angew. Chem., Int. Ed.*, 2020, **59**, 9288–9292.

82 D. Mao, D. Kong, F. Hu, Kenry, G. Qi, S. Ji, W. Wu and B. Liu, One-step in vivo metabolic labeling as a theranostic approach for overcoming drug-resistant bacterial infections, *Mater. Horiz.*, 2020, **7**, 1138.

83 E. Y. Yu, M. M. S. Lee, J. H. C. Chau, K. W. K. Lam, H. Park, R. T. K. Kwok, J. W. Y. Lam, Y. Li and B. Z. Tang, One-step light-up metabolic probes for in situ discrimination and killing of intracellular bacteria, *Mater. Chem. Front.*, 2022, **6**, 450–458.

84 M. M. S. Lee, D. Yan, J. H. C. Chau, H. Park, C. C. H. Ma, R. T. K. Kwok., J. W. Y. Lam, D. Wang and B. Z. Tang, Highly efficient phototheranostics of macrophage-engulfed Gram-positive bacteria using a NIR luminogen with aggregation-induced emission characteristics, *Biomaterials*, 2020, **261**, 120340.

85 T. Dai, B. Guo, G. Qi, S. Xu, C. Zhou, G. C. Bazan and B. Liu, An AIEgen as an intrinsic antibacterial agent for light-up detection and inactivation of intracellular Gram-positive bacteria, *Adv. Healthcare Mater.*, 2021, **10**, 2100885.

86 M.-Y. Wu, J.-K. Leung, C. Kam, T. Y. Chou, J.-L. Wang, X. Zhao, S. Feng and S. Chen, A near-infrared plasma membrane-specific AIE probe for fluorescence lifetime imaging of phagocytosis, *Sci. China: Chem.*, 2022, **65**, 979–988.

87 G. Qi, F. Hu, Kenry, L. Shi, M. Wu and B. Liu, An AIEgen-peptide conjugate as a phototheranostic agent for phagosome-entrapped bacteria, *Angew. Chem., Int. Ed.*, 2019, **58**, 16229–16235.

88 M. Wu, W. Wu, Y. Duan, X. Liu, M. Wang, C. U. Phan, G. Qi, G. Tang and B. Liu, HclO-activated fluorescence and photosensitization from an AIE nanoprobe for image-guided bacterial ablation in phagocytes, *Adv. Mater.*, 2020, **32**, 2005222.

